Winter season Southern Ocean distributions of climate-relevant trace gases

Li Zhou[1], **Dennis Booge**[1], **Miming Zhang**[2], and **Christa A. Marandino**[1]

[1]Research Division 2: Marine Biogeochemistry, GEOMAR Helmholtz Centre for Ocean Research Kiel, Kiel, Germany
[2]Key Laboratory of Global Change and Marine-Atmospheric Chemistry,
Third Institute of Oceanography, Ministry of Natural Resources (MNR), Xiamen, PR China

Correspondence: Li Zhou (lzhou@geomar.de) and Miming Zhang (zhangmiming@tio.org.cn)

Abstract. Climate-relevant trace gas air–sea exchange exerts an important control on air quality and climate, especially in remote regions of the planet such as the Southern Ocean. It is clear that polar regions exhibit seasonal trends in productivity and biogeochemical cycling, but almost all of the measurements there are skewed to summer months. If we want to understand how the Southern Ocean affects the balance of climate through trace gas air–sea exchange, it is essential to expand our measurement database over greater temporal and spatial scales, including all seasons. Therefore, in this study, we report measured concentrations of dimethylsulfide (DMS, as well as related sulfur compounds) and isoprene in the Atlantic sector of the Southern Ocean during the winter to understand the spatial and temporal distribution in comparison to current knowledge and climatological calculations for the Southern Ocean. The observations of isoprene are the first in the winter season in the Southern Ocean. We found that the concentrations of DMS from the surface seawater and air in the investigated area were 1.03 ± 0.98 nmol^{-1} and 28.80 ± 12.49 pptv, respectively. The concentrations of isoprene in surface seawater were 14.46 ± 12.23 pmol^{-1}. DMS and isoprene fluxes were 4.04 ± 4.12 µmol m^{-2} d^{-1} and 80.55 ± 78.57 nmol m^{-2} d^{-1}, respectively. These results are generally lower than the values presented or calculated in currently used climatologies and models. More data are urgently needed to better interpolate climatological values and validate process-oriented models, as well as to explore how finer measurement resolution, both spatially and temporally, can influence air–sea flux calculations.

1 Introduction

Despite the low abundance of trace gases in the atmosphere, their strong chemical reactivity and interactions with radiation have an important influence on air quality and the climate system (Monson and Holland, 2001). For example, a wide variety of trace gases, such as carbon dioxide (CO_2), methane, and nitrous oxide, trap heat and contribute to global atmospheric warming (Liss, 2007). The ocean plays an important role in regulating the sources and sinks of trace gases and, thus, strongly impacts the biogeochemical cycles and budget of reactive trace gases in the global atmosphere (Houghton et al., 2001; Liss et al., 2014; Vallina and Simó, 2007). Studying the air–sea exchange of climate-relevant trace gases can improve the understanding of their effect on climate (Emerson et al., 1999; Liss et al., 2014). Here we focus not only on two typical marine biogenic gases, i.e., dimethylsulfide (DMS) and isoprene, which have a significant influence on aerosols and climate in remote areas of the world (Carpenter et al., 2012; Lovelock et al., 1972) but also on two related sulfur compounds, i.e., dimethylsulfoniopropionate (DMSP) and dimethylsulfoxide (DMSO).

DMS was hypothesized to influence climate by regulating aerosols and clouds, thus, decreasing the amount of solar radiation reaching Earth's surface, known as the CLAW hypothesis (Charlson et al., 1987). DMS is produced from the degradation of DMSP, which is formed in the cells of marine organisms (Cantoni and Anderson, 1956; Curson et al., 2011). DMSP producers include phytoplankton (e.g., coccolithophores, dinoflagellates, diatoms), angiosperms, macroalgae, and some corals (Broadbent et al., 2002; Keller et al.,

1989; Otte et al., 2004; Van Alstyne, 2008; Yoch, 2002). DMSP is cleaved to DMS by bacteria and phytoplankton (Curson et al., 2011; Stefels et al., 2007). DMS produced in the surface ocean can be consumed in the ocean, be oxidized to form DMSO, or be released to the atmosphere (Vogt and Liss, 2009). Only about 10 % of the DMS produced in the surface ocean is released into the atmosphere (Archer et al., 2001). DMS in the atmosphere is oxidized to form sulfuric acid and methanesulfonic acid (McArdle et al., 1998) by hydroxyl radicals (OH; 66 %), nitrate (NO_3; 16 %), and bromine monoxide radicals (BrO; 12 %) globally (Chen et al., 2018), with an atmospheric lifetime of approximately 1 d (Kloster et al., 2006). These DMS byproducts can form aerosols (new particles) (Kulmala et al., 2000) or lead to growth of existing aerosol particles (Andreae and Crutzen, 1997; von Glasow and Crutzen, 2004), aiding the formation of cloud condensation nuclei (CCN) (Charlson et al., 1987; Sanchez et al., 2018). Especially in the remote marine boundary layer (MBL) of the North Atlantic and polar oceans (e.g., the Southern Ocean; SO), DMS-derived non-sea salt sulfate particles account for 33 % and 7 %–65 % (7 %–20 % in winter and 43 %–65 % in summer), respectively (Jackson et al., 2020; Korhonen et al., 2008; Sanchez et al., 2018). Mahmood et al. (2019) show that the mean cloud radiative forcing in the Arctic could increase between 108 % and 145 % from 2000 to 2050 because of increasing Arctic DMS emissions. The global radiative effect of DMS is calculated to be -1.69 to $-2.03\,\mathrm{W\,m^{-2}}$ at the top of the atmosphere (Fiddes et al., 2018; Mahajan et al., 2015; Thomas et al., 2010). These previous studies clearly show the importance of DMS emissions and related atmospheric oxidation products and point to the importance of understanding how global DMS concentrations and subsequent emissions vary over the course of the year and over longer time periods.

Isoprene is the most important biogenic volatile organic compound (BVOC) in the atmosphere, accounting for 50 % of all BVOC emissions coming from terrestrial ecosystems (Guenther et al., 2012; Laothawornkitkul et al., 2009; Sharkey et al., 2008). It impacts the climate system and oxidant chemistry in the atmosphere via secondary organic aerosol (SOA) formation and interaction with OH and the ozone cycle (Claeys et al., 2004; Guenther et al., 1995; Went, 1960). Most isoprene in the atmosphere is produced by terrestrial ecosystems (> 99 %, Guenther et al., 2006), but isoprene is also known to be produced in the ocean as well by different species of phytoplankton, seaweed (Shaw et al., 2003; Bonsang et al., 1992), and some species of marine bacteria (Exton et al., 2013). Since atmospheric isoprene in remote regions of the open ocean are directly related to surface seawater isoprene concentrations (Bonsang et al., 1992), biological marine isoprene production directly influences the magnitude of emissions to the atmosphere. The global marine flux of isoprene is reported to range from 0 to $11\,\mathrm{Tg\,C\,yr^{-1}}$ (Booge et al., 2016), with more extreme values reported by Tran et al. (2013) and Kameyama et

al. (2014) of 0.51–$16.53\,\mathrm{Tg\,C\,yr^{-1}}$ in June–July 2010 in the Arctic and 9.05–$34.96\,\mathrm{Tg\,C\,yr^{-1}}$ in the productive Southern Ocean during austral summer 2010/11, respectively. Despite these values being significantly less than the terrestrial flux (400–$600\,\mathrm{Tg\,C\,yr^{-1}}$; Arneth et al., 2008; Arnold et al., 2009; Baker et al., 2000; Guenther et al., 2006), emitted isoprene in the marine atmosphere plays an important role in the chemistry locally, as it is extremely short-lived (lifetime of $\sim 1\,\mathrm{h}$ due to reaction with OH radicals). Terrestrial isoprene is unlikely to reach the marine boundary layer, and all the marine isoprene emitted will quickly react (Booge et al., 2018; Palmer and Shaw, 2005), influencing local climate and air quality (Claeys et al., 2004).

The fluxes of marine-derived trace gases are an important parameter in atmospheric budgets and for the evaluation of their climate implications. Typically, ocean–atmosphere fluxes are calculated by multiplying the wind-speed-based gas transfer velocity by the bulk phases of the air–sea concentration difference as follows: $F = k\Delta C$ (Liss and Slater, 1974; see "Methods" section below). Often, only seawater concentrations are used, and the atmospheric values are set either to zero or to a constant level, but this can lead to large uncertainties in calculated fluxes (Lennartz et al., 2017; Zhang et al., 2020). Thus, having accurate, repeated measurements of trace gases in the surface ocean, as well as in the marine boundary layer, over a range of spatial and temporal scales is necessary for high-quality flux computations.

The Global Surface Seawater DMS Database contains 89 324 measurements of surface ocean DMS concentration from 1972 to 2019 (https://saga.pmel.noaa.gov/dms/, last access: 23 January 2022). Concentrations of oceanic DMS within the database range between 0 and $295\,\mathrm{nmol\,L^{-1}}$. The broader Southern Ocean (latitude range: 35 to 75° S) is represented by 21 580 points for all seasons, but only 158 points (0.7 %) are from the austral winter. All three DMS climatologies draw heavily on this database (Hulswar et al., 2022; Kettle et al., 1999; Lana et al., 2011). This DMS data product and resulting climatologies, along with those for other trace gases (MEMENTO, MarinE MethanE and NiTrous Oxide; SOCAT, Surface Ocean CO_2 Atlas; HalOcAt, Halocarbons in the Ocean and Atmosphere; among others), are extremely important for model input and validation. If the data products contain the appropriate data, they can resolve seawater concentrations spatially and temporally (e.g., seasonally), as well as begin to point to interannual variability and trends. Therefore, these valuable assets must be equipped with as much data from all regions and seasons as possible. Lana et al. (2011), the most currently used DMS climatology, show that DMS concentrations typically range from 1–$7\,\mathrm{nmol\,L^{-1}}$, with higher concentrations occurring in the high-latitude regions with strong seasonality. The highest DMS concentrations appear in the high-latitude provinces of the North Atlantic and North Pacific in summer, with DMS concentrations generally increasing with temperature and light and sometimes exceeding $20\,\mathrm{nmol\,L^{-1}}$ (Lana et al., 2011). In

the temperate and subtropical provinces, the seasonality becomes weaker, until around the Equator, where there is no obvious seasonal change. The transition to the southern subtropical zone shows weaker seasonal changes, but in austral summer, the Southern Ocean circumpolar regions display a hotspot of DMS concentrations ($> 10 \, \text{nmol L}^{-1}$) (McTaggart and Burton, 1992). Lana et al. (2011; abbreviated as Lana below) estimated that approximately 28.1 Tg S are transferred from the oceans into the atmosphere annually in the form of DMS. The natural sulfur emission has been estimated as 38–89 Tg S yr^{-1} (Andreae, 1990), of which marine DMS emission contributes 30 %–70 %. Although there were many field campaigns performed, the obtained oceanic DMS data are still insufficient, leaving uncertainties about sea-to-air DMS fluxes, especially during the winter season. In the Lana climatology, Southern Ocean data are skewed to spring and summer and are spatially non-uniform, requiring the use of interpolation/extrapolation techniques. Thus, it is unavoidable that large discrepancies between fluxes calculated in situ vs. those in the climatology are found (even at levels as high as 47 %–76 %, Zhang et al., 2020). Better spatial and temporal coverage of in situ measurements are needed for adequate computations of the influence of DMS on global climate.

Marine production and emission of isoprene were first described by Bonsang et al. (1992). Currently published isoprene seawater values from the world oceans generally range from below 1 to 200 pmol L^{-1} (Baker et al., 2000; Bonsang et al., 1992; Booge et al., 2016; Broadgate et al., 1997, 2004; Hackenberg et al., 2017; Li et al., 2019; Matsunaga et al., 2002; Milne et al., 1995; Ooki et al., 2015; Zindler et al., 2014). The highest reported concentration of isoprene, 541 pmol L^{-1}, in the surface ocean was found in the Arctic Ocean in June–July 2010 (Tran et al., 2013). Marine isoprene concentrations in the eastern North Pacific range from 2 to 6.5 pmol L^{-1}, which is at the lower end compared to the world oceans (Moore and Wang, 2006). Additionally, concentrations of marine isoprene show strong seasonal changes in regions with strong seasonal variations in phytoplankton abundances, e.g., in the East China Sea (Li et al., 2018). Booge et al. (2016) improved the predictive capability of the earlier model from Palmer and Shaw (2005) by using isoprene production rates that depend on phytoplankton functional type, but the model is still limited, as it cannot resolve changes in isoprene emissions on short timescales of hours or days. Additionally, the model is validated with a very sparse dataset presently, which cannot resolve seasonal changes in isoprene concentrations for the world oceans. Especially in the Southern Ocean, which is thought to be a hotspot of trace gas emissions during austral summer, data are limited. There are no observations during winter published for this area. Therefore, it is of fundamental importance to increase the dataset of marine isoprene concentrations to understand the magnitude of the influence of marine isoprene emissions on atmospheric processes over the Southern Ocean.

The Southern Ocean is a typical high-nutrient and low-chlorophyll area due to iron limitation, which exerts a strong influence on global biogeochemical cycles and air–sea gas fluxes (Hauck et al., 2013; Zhang et al., 2017). Knowledge of the general biological productivity and circulation patterns of the area has made great advances; however, it is still difficult to resolve the small-scale dynamics of gases in the surface (Tortell and Long, 2009), especially during the wintertime. If we want to understand how the Southern Ocean effects on the balance of climate through trace gas air–sea exchange, it is essential to expand our measurement database over greater temporal and spatial scales, including all seasons. Therefore, in this study we measured the concentrations of DMS; its precursor, DMSP, and oxidation product, DMSO; and isoprene in the Southern Ocean during the austral winter season to gain information on the spatial and temporal distribution in comparison to current knowledge and climatological calculations for the Southern Ocean.

2 Methods

2.1 Cruise description

The measurements were performed on the Southern oCean seAsonaL Experiment (SCALE) cruise aboard the *S. A. Agulhas II*. The cruise started from Cape Town, Republic of South Africa (RSA), on 18 July 2019 (199th day of year, DOY 199), crossed the Southern Ocean to the ice edge, and returned from the ice area on 28 July 2019 (DOY 209) to dock in Cape Town on 11 August 2019 (DOY 223) via the East London port from 7–10 August 2019 (DOYs 219–222) (33–58° S, 2° W–26° E, Fig. 1). Wind speeds ranged between 1.2 and 29.4 m s^{-1} over the cruise. Air mass back trajectories show that the air was of oceanic origin for most of the cruise. Air temperatures ranged from -19.5 to $+18 \, °C$; sea surface temperatures (SSTs) were from -1.8 to $+20.4 \, °C$; and salinity was 19.4–35.3 over the cruise track.

2.2 Sampling

Discrete surface seawater samples for DMS and isoprene were taken bubble-free using transparent 60 mL glass vials (Chromatographie Handel Müller, Fridolfing, Germany) from the underway pump supply. The water samples were kept in a dark, insulated box and analyzed within 2 h. After analysis, DMSP was converted into DMS using sodium hydroxide (NaOH) pellets ($\geq$ 99 %, Carl Roth™ GmbH, Karlsruhe, Germany) and stored for DMSP and DMSO measurements back in the onshore lab.

Our sampling frequency for DMS and isoprene was one sample per hour at the beginning of the cruise. We changed to one sample per 30 min during the last 2 d of the cruise because the concentrations of DMS and isoprene were more variable in the coastal area. DMSP–DMSO samples were taken every 2 h. We obtained 384 discrete samples of DMS
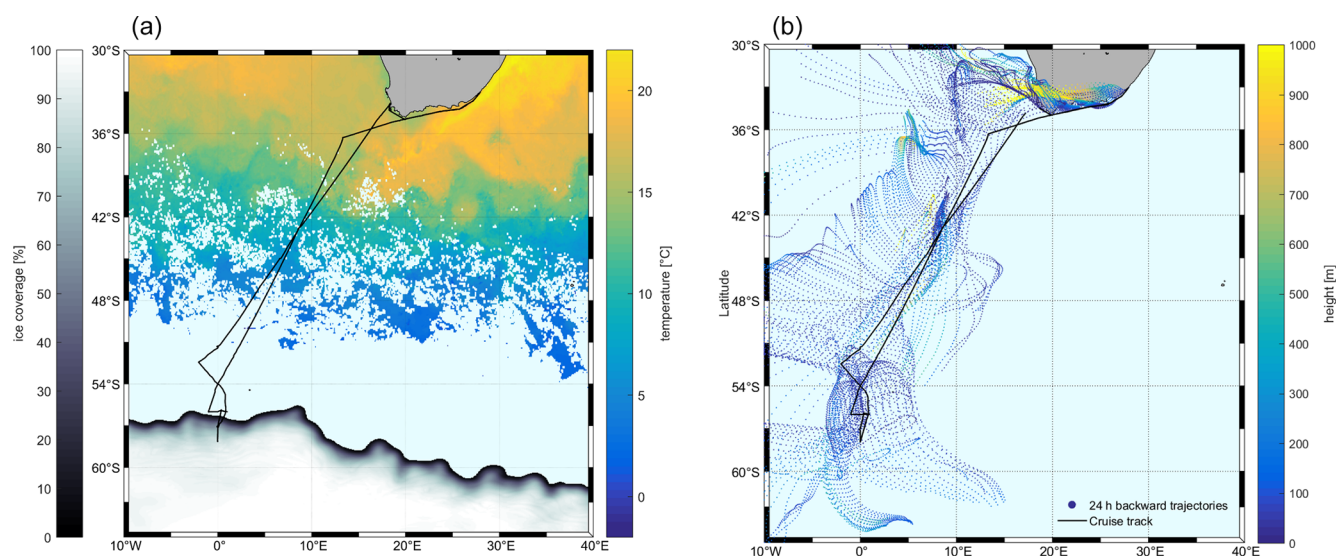
Figure 1. The cruise track (black) superimposed on satellite data. **(a)** Sea surface temperature (SST) and ice coverage (%). SST and sea ice data are derived from satellite (12 July to 12 August 2019; SST – Naval Oceanographic Office, 2008; sea ice data – UK Met Office, 2012.); **(b)** 24 h air mass back trajectories starting at 50 m height from HYbrid Single-Particle Lagrangian Integrated Trajectory (HYSPLIT) using the meteorological fields from the National Centers for Environmental Prediction Global Data Assimilation System (NCEP GDAS). The color shows the average height of the trajectory.

and isoprene and 204 samples of DMSP–DMSO during the cruise. During the cruise, the seawater pumping system was stopped due to the presence of sea ice on 27–28 July 2019 (DOYs 208–209) and while in port of East London (7–10 August 2019, DOYs 219–222), resulting in periods with missing data.

We also performed continuous shipboard underway measurements of surface water and lower-atmospheric DMS using a homemade purge-and-trap sampler coupled with a time-of-flight mass spectrometer system (TOF-MS 3000, Guangzhou Hexin Instrument Co., Ltd., China) (Zhang et al., 2019). Seawater and air samples were introduced continuously to the system through the ship's seawater pump system and air sampler inlet located at the bow at approximately 18 m above the sea surface. A black antistatic tube (1/4 in. o.d., 95 m) was used to transport the air sample to the laboratory. Every 10 min, we obtained a pair of DMS data points (one in seawater and one in the atmosphere). For seawater sample measurements, we purged a 5 mL aliquot with 65 mL min^{-1} of high-purity nitrogen (N$_2$) for 5.5 min. For atmospheric DMS measurements, the air sample was trapped under the mean flow at 65 mL min^{-1} for 3.5 min. The concentrated air sample was injected to the TOF-MS system; then 2 min later the concentrated water sample was injected to the TOF-MS system. The atmospheric and seawater DMS limits of detection (LODs) were 32 pptv and 0.07 nmol L^{-1}, respectively.

2.3 Analysis

DMS, DMSP, DMSO, and isoprene were analyzed by gas chromatography–mass spectrometry (GC–MS) coupled to a purge-and-trap system. Headspace within each sample was made by injecting 10 mL of helium into the vial. Isoprene was fully removed from the remaining 50 mL sample (> 99 %) with helium at a flow rate of 70 mL min^{-1} for 15 min at room temperature (RT). Purge efficiency for DMS was less than 100 % and dependent on the seawater temperature, but the data were corrected for this effect (Fig. S1). Gaseous deuterated isoprene (isoprene-d5; 98 %) was used as internal standard and injected through a 500 µL Sulfinert® stainless-steel sample loop (1/16 in. o.d., Restek, Bad Homburg, Germany). The sample flow was dried using a Nafion® membrane dryer (counter flow: N$_2$, 180 mL min^{-1}, Perma Pure, Ansyco GmbH, Karlsruhe, Germany). After purging, DMS and isoprene were trapped in a Sulfinert® stainless-steel trap cooled with liquid N$_2$. The sample was injected into the GC by immersion in hot water. Retention times for DMS and isoprene (m/z: 61, 62; 67, 68) were 5.0 and 5.3 min. For analysis of DMSP, 10 mL of the DMS sample was transferred to brown glass vials (Chromatographie Handel Müller, Fridolfing, Germany). After the DMSP analysis, DMSO was converted into DMS by adding cobalt-dosed sodium borohydride (NaBH$_4$) (90 %, Sigma-Aldrich Chemie GmbH, Taufkirchen, Germany) and analyzed immediately with the same technique as mentioned above. Liquid standards and an internal standard were used to calibrate the system for DMS and isoprene every day during the analysis

on board. Liquid calibrations were performed every measuring day for the DMSP–DMSO analysis in the lab. The given LODs of this system are 10 times the standard deviation of the baseline noise, which are 1.8×10^{-13} and 5.5×10^{-13} mol for DMS and isoprene, respectively.

Continuous underway measurements of SST and salinity, as well as wind speed and direction, air temperature, pressure, and global radiation, were recorded from the ship's pumped seawater supply and the meteorological tower, respectively.

2.4 Calculation of air–sea flux

The air–sea fluxes of all gases were calculated with Eq. (1):

$$F = (1 - A)k \cdot \Delta C = (1 - A)k \cdot \left(\mathrm{Cw} - \frac{C_\mathrm{a}}{H} \right), \tag{1}$$

where F is the flux (per mass area per time), A is fraction of sea surface covered by ice, ΔC is the concentration difference between air (C_a) and water (Cw), k is the gas exchange coefficient (m s^{-1}) in water (Liss and Slater, 1974), and H is the Henry's law coefficient used to calculate gas solubility. The gas exchange coefficient for the gases of interest is usually approximated as the water–air side transfer velocity, k_w. We use the following parametrizations derived from dual tracer (Nightingale et al., 2000; N00) and eddy covariance direct measurement of air–sea DMS transfer (Zavarsky et al., 2018; Z18) to calculate the DMS gas transfer velocity following Eqs. (2) and (3):

$$k_{\mathrm{DMS,N00}} = \left(0.222 \cdot U^2 + 0.333 \cdot U \right) \left(\frac{Sc}{660} \right)^{-0.5}, \tag{2}$$

$$k_{\mathrm{DMS,Z18}} = (2.00 \cdot U + 0.94) \left(\frac{Sc}{660} \right)^{-0.5}. \tag{3}$$

We use the Wanninkhof (1992; W92) and Wanninkhof (2014; W14) formulations, based on a synthesis of tracer, wind–wave tank, radon, and radiocarbon studies to determine k_{isoprene} (Eqs. 4 and 5):

$$k_{\mathrm{isoprene,W92}} = 0.31 \cdot U^2 \left(\frac{Sc}{660} \right)^{-0.5}, \tag{4}$$

$$k_{\mathrm{isoprene,W14}} = 0.251 \cdot U^2 \left(\frac{Sc}{660} \right)^{-0.5}, \tag{5}$$

where U is the wind speed at 10 m height and Sc is the Schmidt number. The wind was measured at 18 m height and converted to 10 m using

$$\frac{U_x}{U_{10}} = \left(\frac{Z_x}{Z_{10}} \right)^P, \tag{6}$$

where U_x is the observed wind speed at 18 m; Z_x and Z_{10} are heights of 18 and 10 m, respectively; and P depends on atmospheric stability and underlying surface characteristics

and is set to 0.11 (Hsu et al., 1994). Sc is defined as the ratio of the kinematic viscosity of water to the diffusion coefficient of gas in water, and 660 represents CO_2 in seawater at 20 °C. We estimate Sc of DMS and isoprene following Wanninkhof (2014) and Palmer and Shaw (2005), respectively:

$$Sc_{\mathrm{DMS}} = 2855.7 - 177.63\, T_\mathrm{c} + 6.0438\, T_\mathrm{c}^2$$
$$\qquad - 0.11645\, T_\mathrm{c}^3 + 0.00094743\, T_\mathrm{c}^4, \tag{7}$$

$$Sc_{\mathrm{isoprene}} = 3913.15 - 162.13\, T_\mathrm{c} + 2.67\, T_\mathrm{c}^2$$
$$\qquad - 0.012\, T_\mathrm{c}^3, \tag{8}$$

where T_c is SST (°C).

In addition, for DMS, the partitioning of the gas transfer coefficient between air-side and water-side control (γ_a) can change due to low SSTs and from moderate wind speeds (McGillis et al., 2000). Thus, we consider both water-side and air-side control when calculating DMS fluxes:

$$F = (1 - A)\, k_w (1 - \gamma_\mathrm{a}) \cdot \Delta C, \tag{9}$$

where A is the fraction of sea ice cover and γ_a is calculated as

$$\gamma_\mathrm{a} = \frac{1}{1 + \frac{k_\mathrm{a}}{\alpha k_w}}, \tag{10}$$

where k_a is air-water side transfer coefficient and α is the Ostwald solubility coefficient. These parameters were calculated as described in McGillis et al. (2000) and the references therein as

$$k_\mathrm{a} \approx 659 U_{10} \left(\frac{M}{M_{\mathrm{H_2O}}} \right)^{-0.5}, \tag{11}$$

$$\alpha = e^{\left[\frac{3525}{T(\mathrm{K})} - 9.464 \right]}, \tag{12}$$

where M is the molecular weight of DMS or H_2O and T is the seawater temperature (K). Finally, as no atmospheric measurements of isoprene were obtained, we assume C_a of isoprene is zero in the remote MBL due to its very short lifetime. Two wind-speed-based gas transfer parameterizations for each gas were used, and the respective fluxes were compared to each other and to existing climatologies or model calculations. For DMS, N00 was used for direct comparison to the Lana climatology and Z18 because it is known that DMS exhibits mostly interfacial gas transfer, which is more accurately described with a linear wind speed dependence. For isoprene, we used parameterizations with a quadratic dependence on wind speed, since it is less soluble than DMS and likely to have more influence from bubble-mediated gas transfer. W92 was chosen for direct comparison with Palmer and Shaw (2005) and Booge et al. (2016), but the more accurate version of this parameterization is W14, and, thus, it was also used for comparison.

2.5 Data analysis

The data were tested for normal distribution using the Kolmogorov–Smirnov test and was determined to be non-normally distributed. Outliers were identified as deviating more than 3 times from the standard deviation of the mean. We used Spearman correlation analysis to identify correlation coefficients between DMS, DMSP, and DMSO. The F statistic, p value (significance), R (correlation coefficient), and R^2 (variance proportionality) were calculated to test for a linear correlation between two variables. All statistical analyses were performed using MATLAB (The MathWorks, Inc., Natick, Massachusetts, United States).

3 Results and discussion

3.1 Comparison of DMS measurements by GC–MS and TOF-MS

Simultaneous measurements of surface seawater DMS concentrations during SCALE were performed using both the GC–MS and TOF-MS systems. We ensured method comparability by using the same DMS standards (both gas and liquid) on board. We collected 361 GC–MS samples and 2245 TOF-MS samples during the in situ observations. Although the detection limit of the GC–MS system is lower than that of the TOF-MS system, the time resolution of the TOF-MS system is higher. Considering the different time resolution of the two instruments, we only compare the data of samples taken at the same time (258 data points). The datasets were found to be correlated and agreed well with each other (Fig. 2a, $p < 0.01$, slope $= 0.91$, $R = 0.67$). The median and mean values of TOF-MS observations are higher, 42.5 % and 12.9 %, respectively, than those by GC–MS (Fig. 2b). This may be due to the fact that the TOF-MS system does not have a column that separates isomers and cannot distinguish between compounds of the same mass number, making the mean and median values higher than GC–MS. Alternatively, we observed that 95 % of the DMS concentrations in both instruments were less than 1.7 nmol L^{-1} and that in this concentration range, the slope of the fit is slightly lower than the 1 : 1 line. This may reflect added uncertainty from the GC–MS purge efficiency correction. The regions of the cruise track corresponding to these lower concentrations were the coldest regions encountered, corresponding to the highest solubilities. Thus, the GC–MS values may be too low in this concentration range. As it is not clear which set of measurements were incorrect and given the very good agreement, we decided to use the data in following way: fluxes were computed over the entire cruise track, using GC–MS measurements for seawater DMS concentrations, as the same instrument was used to perform DMSP and DMSP measurements. TOF-MS measurements were used for atmospheric mixing ratios.
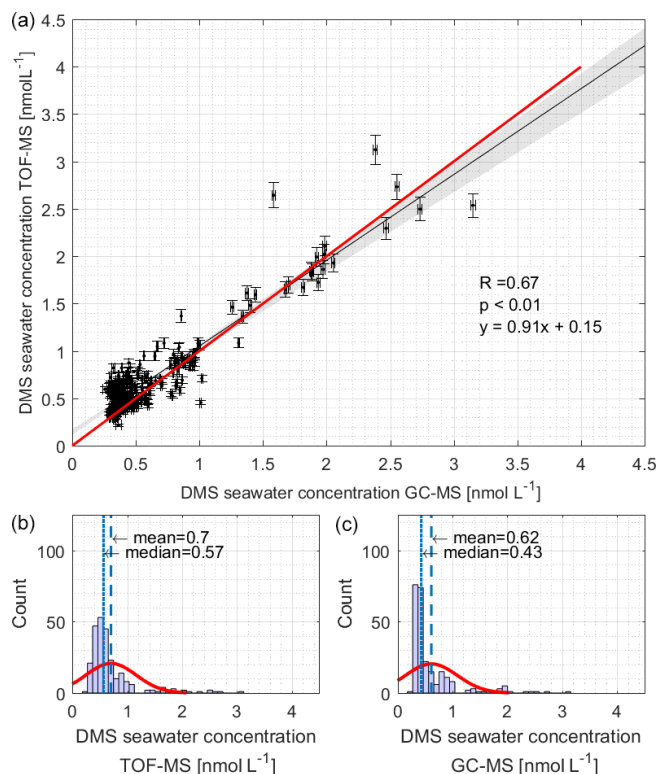

Figure 2. The (a) correlation and (b, c) Gaussian distribution analysis of DMS concentrations measured by TOF-MS (b) and GC–MS (c). TOF-MS data were matched to GC–MS data within a ±5 min timing interval. The black line and red line in (a) denote the regression line and the 1 : 1 line, respectively. The red lines in (b) and (c) denote the density curve.

3.2 Environmental characterization during SCALE

The cruise started in the Atlantic Ocean, at Cape Town, and sailed, crossing different fronts, to the Southern Ocean ice zone before returning along almost the same track, via East London, back to Cape Town (Fig. 1). According to the ratio of SST and salinity along the track, three different regions were identified, namely the subtropical, Antarctic Circumpolar Current (ACC), and Antarctic regions (Fig. 3; see the Supplement for more details on the defining characteristics; Fig. S2). At DOYs 201.91 and 216.01, we observed a change between the ratios greater than 0.05 but did not find such a strong change at other observation points, thus distinguishing the subtropical and ACC regions. For the Antarctic region, we found that the ratio of change intensity was not as strong as between subtropical and ACC but did occur (a change of 0.04). From this ratio, we distinguish the two regions of ACC and Antarctic. Luis and Lotlikar (2021) report that the range of SST in the ACC region is from 1.8 to 9 °C, and that of salinity is from 33.85 to 34.8; the SST of the Antarctic area is less than 1.5 °C, and the salinity is less than 34. These ranges are consistent with our SST–salinity-ratio-defined re-

gions. Unfortunately, in the ice area (DOYs 208.4–209.8), surface seawater was not collected, because the inlet of the underway pump was blocked by the sea ice. The underway pump was shut down also when the ship docked at the port of East London (DOYs 219.4–222.4). The lowest air temperature occurred at DOY 208, which was approximately $-20\,°C$ (Fig. 3c). During the cruise, wind speed (Fig. 3b) was on average $15.0 \pm 2.5\,\mathrm{m\,s^{-1}}$. We experienced higher wind speeds between DOYs 210 and 214 and DOYs 216–217, averaging over $20\,\mathrm{m\,s^{-1}}$. As the ship approached the coast, winds slowed down, and air temperatures rose.

3.3 Distribution of dissolved DMS and related compounds

During the campaign, the mean sea surface concentration of DMS was $1.03 \pm 0.98\,\mathrm{nmol\,L^{-1}}$ using the GC–MS system $(0.75 \pm 0.52\,\mathrm{nmol\,L^{-1}}$, TOF), ranging from 0.26 to $5.18\,\mathrm{nmol\,L^{-1}}$ $(0.21–3.96\,\mathrm{nmol\,L^{-1}}$, TOF, Fig. 4a). The concentrations measured during SCALE are comparable to those from previous winter measurements (Table 1). Measurements made at lower latitudes appear to be consistently higher than those made at higher latitudes. Surface seawater DMS levels in the Southern Ocean during winter were much lower than those measured in spring (e.g., 0.4–7.9 and 3–40 $\mathrm{nmol\,L^{-1}}$, Curran and Jones, 2000; Kiene et al., 2007), summer (e.g., $0.6–30\,\mathrm{nmol\,L^{-1}}$, Tortell and Long, 2009), and autumn (e.g., $0.7–3.3\,\mathrm{nmol\,L^{-1}}$ and not detected (nd) to $27.9\,\mathrm{nmol\,L^{-1}}$, Wohl et al., 2020; Yang et al., 2011; Zhang et al., 2020). The average concentration in the subtropical region was the highest during the entire cruise, which was $1.86 \pm 1.05\,\mathrm{nmol\,L^{-1}}$, while the average concentrations in the ACC and Antarctic regions were significantly lower, 0.48 ± 0.15 and $0.36 \pm 0.04\,\mathrm{nmol\,L^{-1}}$, respectively. The southern and northern ACC transects and the Antarctic regions presented a similar concentration range between 0.26 and $1.00\,\mathrm{nmol\,L^{-1}}$; however, over the two observation periods of the subtropical region, the concentration ranges of DMS were not similar. The subtropical region along the first transect (southwards) exhibited lower concentrations than the same area of the second transect (northwards). This difference could be due to the duration of time spent sampling at the coast: at the beginning of the cruise, the coastal zone was left behind relatively quickly, while on the return trip, a greater period of time was spent sampling the near-shore waters. Fluctuations in DMS concentrations were visible where the subtropical region and the ACC circulation met, along with SST and salinity changes. Finally, in order to understand uncertainties induced by sparse sampling in winter, we compare our data to the Lana climatology (Lana et al., 2011). We have calculated that our values are 2.2 ± 0.4 times lower than the values of Lana et al. (2011) in the open-ocean regions of our cruise track. However, in the coastal area the described values in Lana et al. (2011) is 1.6 ± 1.0 times lower than our measured values in the same area (Fig. 5).

The average sea surface concentration of DMSP during the observation period was $11.26 \pm 6.98\,\mathrm{nmol\,L^{-1}}$, and the distribution range was $3.73–40.27\,\mathrm{nmol\,L^{-1}}$ (Fig. 4b). By comparing to previous research, it can be seen that the concentration during the entire observation period is lower than most of the existing literature values, likely because biological activity in winter is low, resulting in the lowest concentration of DMSP (Curran et al., 1998; Jones et al., 1998; Kiene et al., 2007). The only values that are similarly low are also from the winter season (Cerqueira and Pio, 1999). The highest concentrations were found in the subtropical region (average: $16.48 \pm 7.08\,\mathrm{nmol\,L^{-1}}$). Average concentrations in the ACC and Antarctic regions were 9.00 ± 3.44 and $5.19 \pm 0.94\,\mathrm{nmol\,L^{-1}}$, respectively.

The average sea surface concentration of DMSO during the observation period was $5.41 \pm 5.31\,\mathrm{nmol\,L^{-1}}$, and the distribution range was $1.18–33.56\,\mathrm{nmol\,L^{-1}}$ (Fig. 4b). The subtropical region had the highest average concentration of $9.28 \pm 6.15\,\mathrm{nmol\,L^{-1}}$, and the average concentrations of the ACC and Antarctic regions were similar, 2.74 ± 1.17 and $1.90 \pm 0.52\,\mathrm{nmol\,L^{-1}}$, respectively. Kiene et al. (2007) measured the concentration of dissolved DMSO in the Southern Ocean in the summer of 2009, and the concentration range $(1–55\,\mathrm{nmol\,L^{-1}})$ was higher than the concentration of total DMSO in this study. Our study area was not subject to human interference, and the biological activity, as well as light levels, in winter is low; therefore our wintertime measured concentrations can be regarded as the lowest background value of the area.

3.4 Relationships between sulfur compounds

Correlation analysis of DMS and DMSP–DMSO in different circulation regions (Fig. 6) shows that the regional relationships are different. In the subtropical area, the slopes of DMS against DMSP–DMSO are similar, with p values less than 0.01 and R^2 values higher than 0.5. Studies have shown that DMSO can be a source of DMS in areas with strong sunlight (Zindler et al., 2015). Therefore, in the subtropical area, the source of DMS relates to both DMSP and DMSO. The slope of DMSP against DMSO is 0.64, with a p value less than 0.01 and $R^2 = 0.6$ (Fig. 6c). This information, along with the similar concentration range for both DMSO and DMSP (ca. $40\,\mathrm{nmol\,L^{-1}}$), indicates a tight coupling between DMSP and DMSO. Overall, the positive correlation between DMS, DMSP, and DMSO indicates that there is strong cycling between the three in this region.

We further split the subtropical data into coastal (blue dots, Fig. 6a–c) and open ocean (red dots, Fig. 6a–c), as we see that there is a distinct concentration difference in these subregions. We again analyzed the relationship between DMS, DMSP, and DMSO in these two areas, and we find that the concentration of DMS, DMSP, and DMSO is higher at the coasts than in the open ocean. The R^2 values between DMS and DMSP are 0.81 and 0.38 in open seas and near-
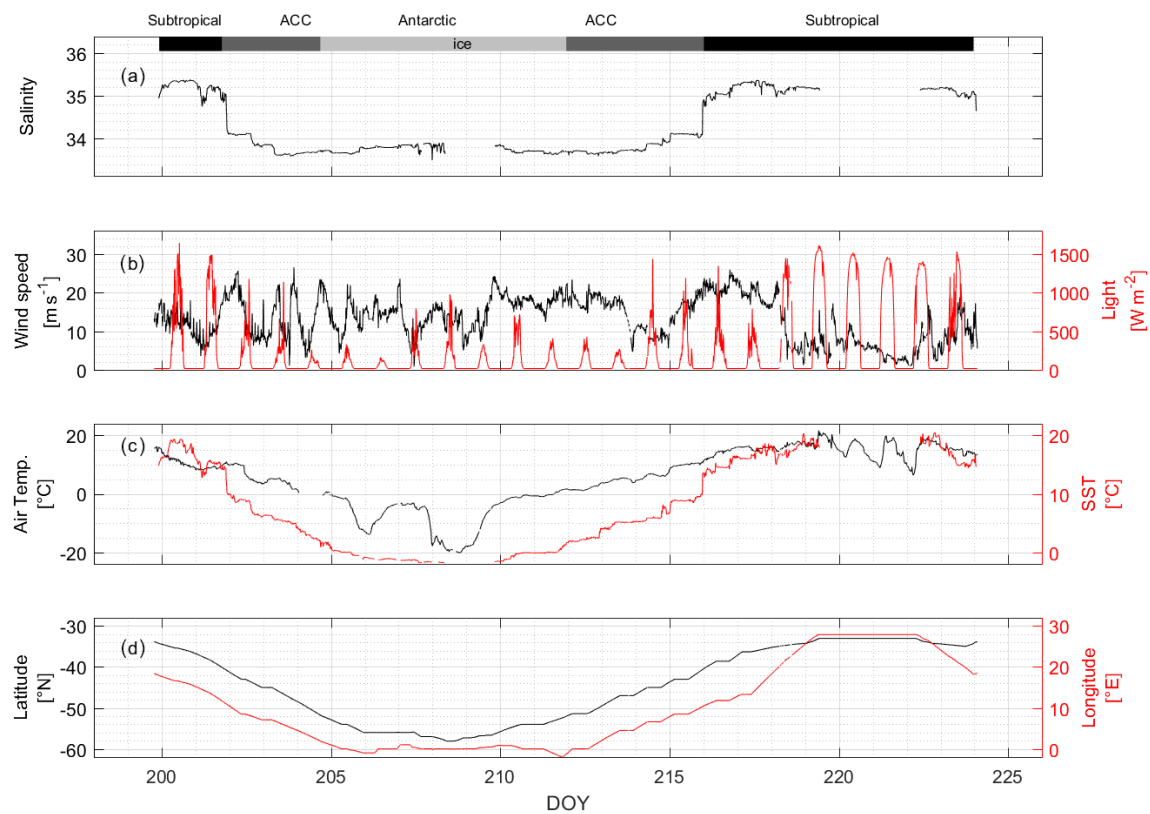
Figure 3. Auxiliary parameters. In situ measurements of (a) salinity, (b) wind speed at 18 m (black) and light levels (red), (c) air temperature (black) and SST (red), and (d) cruise track latitude (black) and cruise track longitude (red) averaged over 10 min. The bars across the top of the figure denote the different hydrographic regions discussed throughout the text.

Table 1. Literature review of published field studies of DMS concentrations and mixing ratios (seawater, air) during wintertime (SO: Southern Ocean; O: open ocean; I: island; C: coastal).

Reference	Area	Water type	DMS_{water} (nmol L^{-1})		DMS_{air} (pptv)	
			Mean	Range	Mean	Range
Lee and De Mora (1996)	New Zealand	O, C	1.82	1.51–2.82		
Nguyen et al. (1992)	Amsterdam Island (Indian Ocean)	C, I	0.20		13.20	
Gibson et al. (1988)	Antarctic	O, C	1.38	1.11–1.64		
Nguyen et al. (1990)	Southern Indian Ocean	O, C	2.51	0.30–2.01	58	34–274
Akademik Korolev (1987), unpublished	Indian and Pacific oceans	O	0.75	0.31–1.25	1.25	
Marion Dufresne (1998), unpublished	Indian Ocean	O	0.96	0.37–2.01	2.01	
This study	SO: whole cruise	O	1.03 ± 0.98	0.26–5.18	28.80 ± 12.49	0.06–88.68
	SO: subtropical region		1.86 ± 1.05	0.45–5.18	23.25 ± 7.16	7.49–35.71
	SO: ACC region		0.48 ± 0.15	0.30–1.00	29.16 ± 9.41	0.06–58.34
	SO: Antarctic region		0.36 ± 0.04	0.26–0.47	31.40 ± 16.77	0.06–88.68

coast areas, and the slopes are 8.14 and 7.13, respectively. The p values are less than 0.01 for both subregions. This result shows that closer to the subtropical coastal area, the DMSP has a positive effect on DMS, with a lesser impact in the open sea. While it has been shown that more microbial DMSP cleavage to DMS occurs at the coast (Zubkov et al., 2002), the relationship between the two compounds may be confounded by DMS interconversion with DMSO (as discussed below). The R^2 values between DMS and DMSO in the open-ocean and the coastal regions are 0.77 and 0.61; the p values are less than 0.01; and the slopes are 3.61 and 6.02, respectively. The obvious difference in correlation and
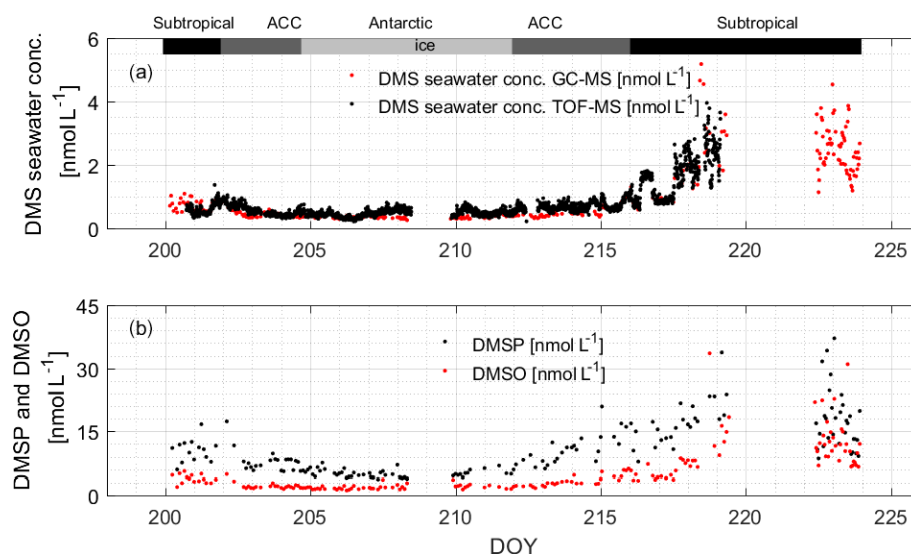
Figure 4. (a) Measured DMS concentrations in seawater using both instruments; **(b)** measured DMSP and DMSO concentrations in the sea surface using the GC–MS system. The bars across the top of the figure denote the different hydrographic regions discussed throughout the text.
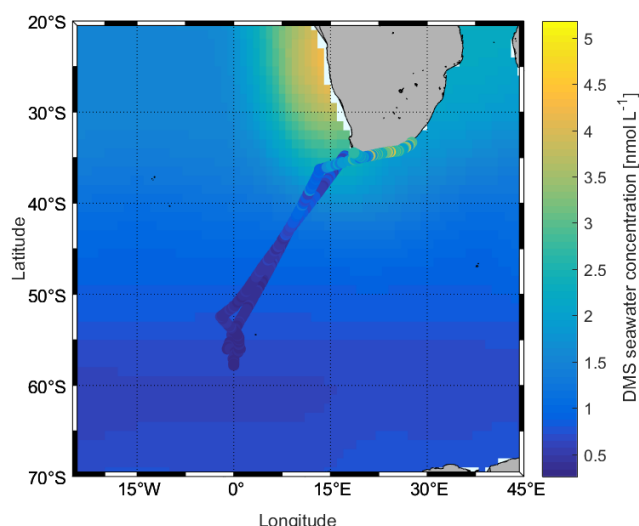

Figure 5. Comparison between measured DMS concentrations (cruise track trace) and those in the Lana et al. (2011) climatology (background) for August.

slope indicates that the relationship is different, possibly because the coastal region may contain more photosensitizers (CDOM, chromophoric dissolved organic matter; FDOM, fluorescent dissolved organic matter) promoting increased photochemical cycling between the two compounds (Mopper and Kieber, 2002). Comparing the relationship between DMSP and DMSO, we find that in the near-coast area, the R^2 value between DMSP and DMSO is 0.50, while in the open sea it is 0.76; the p values are less than 0.01, and the slopes are 0.49 and 0.37, respectively. This may indicate that

DMSO is higher at the coast, not because of direct algal production of DMSO along with DMSP but because there is more DMSP to DMS microbial cleavage (Fig. 6a) and strong cycling between DMS and DMSO due to enhanced photochemistry (Fig. 6b) – where DMSP is high because of greater biological productivity (Hatton et al., 2004, 2012; Stefels et al., 2007).

The concentration range of DMS, DMSP, and DMSO in the ACC region is reduced by half or even more than that of the subtropical area. In addition, it can be seen that the slope (20.1) between DMS and DMSP is significantly higher than that between DMS and DMSO or DMSP and DMSO. The p value is less than 0.01, and the R^2 value is greater than 0.5, indicating that DMSP has a leading role in the generation of DMS. The higher slope means that more DMSP is required in the ACC region to produce DMS compared to the subtropical region. This again may indicate different microbial pathways leading to higher DMS production in the subtropical area.

In the Antarctic circulation area, the p values between DMS and DMSP, DMS, and DMSO are all greater than 0.01, indicating that the sources of DMSP and DMSO are not connected. Although the p value between DMSP and DMSO is less than 0.01, the R^2 value is only 0.17, supporting the idea that the cycling of the compounds is relatively decoupled (Fig. 6, Antarctic region). There appears to be little to no biological activity there. Additionally, due to the low dose of solar radiation during winter in the Southern Ocean (Fig. 3g), little DMSO production via photoreaction from DMS is expected (Vallina and Simó, 2007).

Simó et al. (2000) found that the relationship between DMSPp : DMSOp and SST points to the presence of coccolith blooms that lead to high levels of DMSP. Simó and
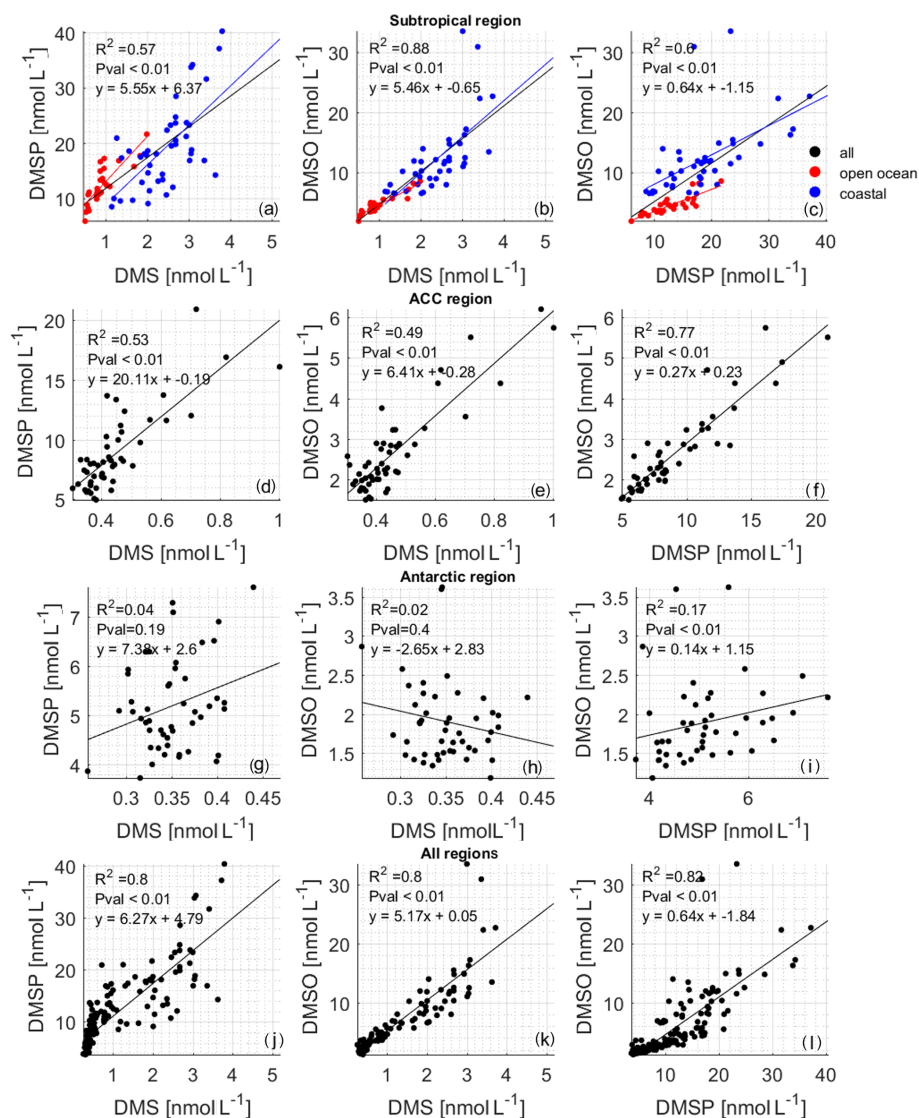
Figure 6. Correlations between measured DMSP and DMS (the left column of the figure), DMSO and DMS (the middle column of the figure), and DMSO and DMSP (the right column of the figure): **(a–c)** subtropical region (black points), **(d–f)** ACC region, **(g–i)** Antarctic region, and **(j–l)** entire cruise. The red points in **(a)**–**(c)** are data from the open ocean in the subtropical area, and the blue points are data from the subtropical area near the coast. The results of the correlation analysis between DMS and DMSP are $R^2 = 0.81$, $p < 0.01$, $y = 8.14x + 5.01$ for open-ocean waters and $R^2 = 0.38$, $p < 0.01$, $y = 7.13x + 1.9$ for coastal waters. The results of the correlation analysis between DMS and DMSO are $R^2 = 0.77$, $p < 0.01$, $y = 3.61x + 1.12$ for open-ocean waters and $R^2 = 0.61$, $p < 0.01$, $y = 6.02x - 2.04$ for coastal waters. The results of the correlation analysis between DMSP and DMSO are $R^2 = 0.76$, $p < 0.01$, $y = 0.37x - 0.11$ for open-ocean waters and $R^2 = 0.5$, $p < 0.01$, $y = 0.49x + 3.26$ for coastal waters.

Vila-Costa (2006) found that the particulate DMSP (DMSPp) and DMSO (DMSOp) ratio has a negative correlation with SST and latitude. Zindler et al. (2013) found that the trend changes sign at temperatures below 5 °C. The temperature in our observation area varies widely, so it is a good dataset for determining if this change in relationship with SST is robust. Unfortunately, we did not measure DMSPp and DMSOp, so we compare total DMSP : DMSO with SST (Fig. 7). Indeed, we find that our data corroborate both studies (Fig. 7, red plus signs; Fig. S3), with an increasing relationship at low temper-

atures until about 5 °C and then a decreasing relationship in warmer waters. The relationship between total DMSP (DM-SPt) and DMS to SST over the entire cruise was also investigated (Fig. S3). The pattern observed in DMSPt : DMSOt associated with SST above 5–10 °C is likely due to the variation in DMSO production rate associated with the change in solar radiation dose. High DMSO production rates coupled to high DMSP degradation rates under high-SST conditions causes a decline in the observed ratio with temperature. The opposite is true in colder waters with corresponding low-light
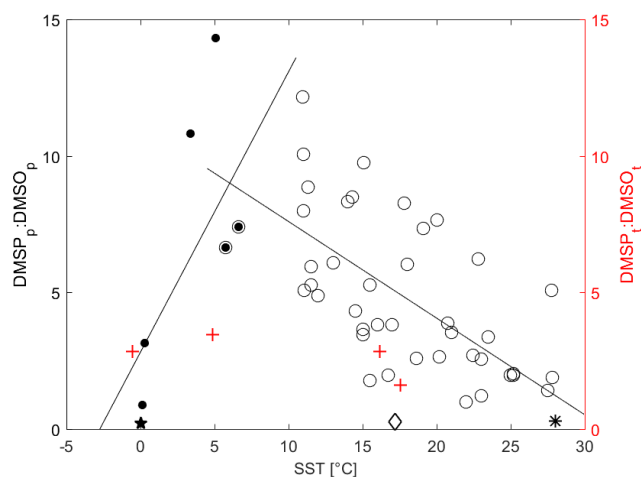
Figure 7. Average DMSPt : DMSOt vs. SST (red) and average DMSPp : DMSOp vs. SST (black). Mean ratios for individual campaigns are recalculated from the data listed in Simó and Vila-Costa (2006). We added data points consisting of the mean DMSPp : DMSOp and SST (given in parenthesis) from the East China Sea (0.27, 17.2 °C, open diamond) (Yang and Yang, 2011), the northern Baffin Bay (0.20, estimated 0 °C; closed pentagram) (Bouillon et al., 2002), and the western Pacific Ocean (0.22, 28 °C, asterisk) (Zindler et al., 2013). The linear correlations are $y = -0.35x + 11.13$ ($R^2 = 0.45$, open circles) and $y = 1.03x + 2.82$ ($R^2 = 0.57$, solid circles). Our Southern Ocean, ACC, and subtropical open-ocean and coastal areas are the red plus signs.

levels (Fig. 3), leading to an increase in the ratio with temperature until around 5 °C. As is discussed in the Supplement in more detail, DMSPt : DMS follows a similar trend as DMSPt : DMSO to SST, which may be due to decreasing DMSP production with temperature and increasing DMSP to DMS microbial cleavage (Stefels et al., 2007; Yoch, 2002).

3.5 DMS atmospheric mixing ratios and fluxes

The average DMS mixing ratio in the boundary layer throughout the observation period was 28.80 ± 12.49 (0.06–88.68) pptv. The averages for each region were 23.25 ± 7.16 (7.49–35.71) pptv, 29.16 ± 9.41 (0.06–58.34) pptv, and 31.40 ± 16.77 (0.06–88.68) pptv in the subtropical, ACC, and Antarctic regions, respectively. These values fall within the range of previously reported winter atmospheric mixing ratios over the Southern Ocean (Table 1), which are lower than those reported for spring (nd–755 pptv, Inomata et al., 2006) and autumn (nd–3900 pptv, Zhang et al., 2020). The temporal trends of atmospheric DMS mixing ratios during our research campaign were different from those observed in seawater (Fig. 8c). For example, the highest atmospheric concentrations of DMS were found in the Antarctic region, where seawater concentrations were the lowest. The likely reasons for this include lower atmospheric photochemical reaction rates, a lower boundary layer, and DMS release from ice (Koga et al., 2014). The lower reaction rates result

in an increased lifetime of DMS and a buildup of DMS in the boundary layer. Low sea surface temperatures create a lower atmospheric boundary layer during winter, which aids in DMS buildup. Finally, it has been shown that when research vessels travel in the ice area and crush the ice, higher concentrations of DMS can be released from the gap between the ice and the sea surface, which also increases the concentration of DMS in the air (Koga et al., 2014).

DMS fluxes were calculated using two different gas exchange coefficient parameterizations from Zavarsky et al. (2018; Z18) and Nightingale et al. (2000; N00) (Fig. 8b). The Z18 parameterization is based on direct flux measurements of DMS, while the N00 values are from dual tracer studies of ^{3}He / SF$_6$. For our purposes, the Z18 parameterization is preferred, but in order to compare with the Lana climatology, N00 is used as well. It can be seen from the results that kZ18 (17.78 ± 7.30, 0.99–43.48 cm h^{-1}) is lower than kN00 (29.78 ± 20.14, 0.12–131.52 cm h^{-1}) over the wind speed range observed during SCALE. Values of kZ18 are 20.77 ± 9.18 (2.32–43.49), 17.27 ± 5.72 (1.10–38.40), and 14.93 ± 4.00 (0.99–31.22) cm h^{-1} in the subtropical, ACC, and Antarctic regions, respectively. The values of kN00 are 34.18 ± 26.29 (0.37–123.90), 29.67 ± 16.56 (0.12–131.51), and 25.50 ± 11.92 (0.12–100.83) cm h^{-1}, respectively. Especially in areas with high wind speeds (DOYs 216–218), kN00 is significantly higher than kZ18. The difference lies in the wind speed dependency of the two parameterizations: Z18 is linear, while N00 has a quadratic term. This difference in functional form is, likely, because the solubilities of the dual tracer gases and DMS are different, which could lead to discrepancies at high wind speeds where bubble-mediated gas transfer is important (i.e., more soluble gases, such as DMS, have a lower bubble-mediated gas exchange potential). Therefore, the N00 parameterization may not be applicable to DMS fluxes at high winds. However, the difference between kZ18 and kN00 data is not significant from DOYs 219 to 225, which corresponds to the wind speeds below 10 m s^{-1} (Fig. 8a).

The average flux calculated using kZ18 is 4.04 ± 4.12 µmol m^{-2} d^{-1}, and the range is 0.02 to 22.03 µmol m^{-2} d^{-1}. The average calculated flux using kN00 is 6.10 ± 7.08 µmol m^{-2} d^{-1}, and the range is 0.04 to 37.12 µmol m^{-2} d^{-1}. In the subtropical, ACC, and Antarctic regions, the average fluxes (ranges) calculated using kZ18 are 7.63 ± 4.29 (1.00–22.03), 2.00 ± 1.33 (0.21–6.12), and 1.07 ± 0.51 (0.02–2.02) µmol m^{-2} d^{-1}, respectively, while the average fluxes (ranges) calculated using kN00 are 10.88 ± 8.71 (0.67–37.62), 3.53 ± 3.05 (0.06–12.60), and 1.95 ± 1.14 (0.04–5.06) µmol m^{-2} d^{-1}. For areas with high concentrations of DMS in the water and high wind speeds, the computed fluxes using kN00 can be twice as much as those using kZ18 (DOYs 216–218). In areas with high wind speed and low concentrations of DMS in the water, the effect on the calculated flux is not as obvious, despite the difference in k values (e.g., DOY 207), and both computed
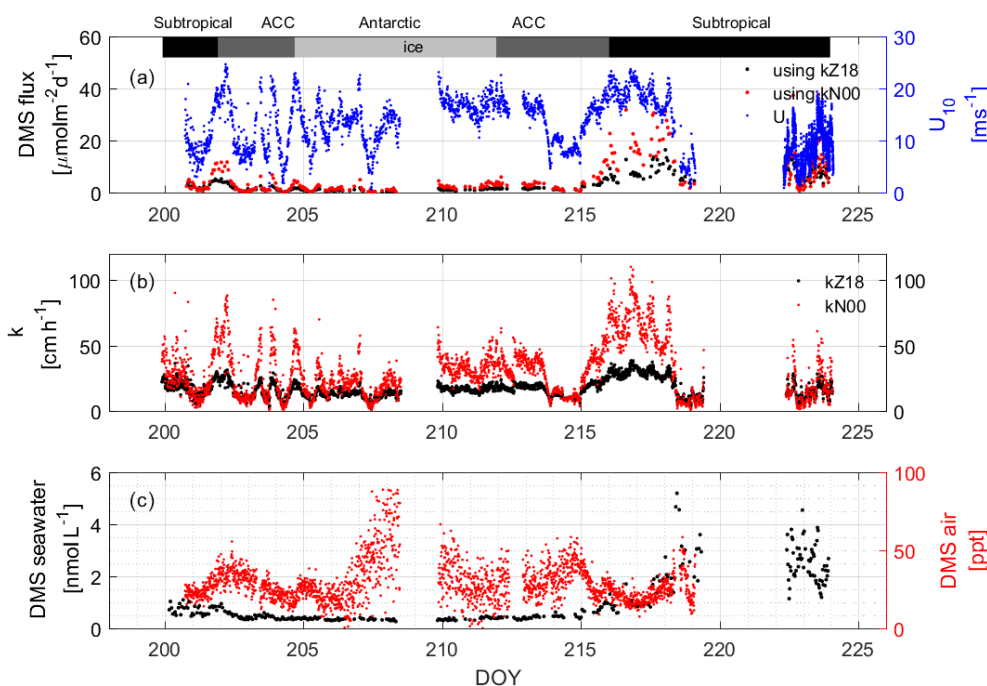
Figure 8. (a) Calculated DMS fluxes that depend on the indicated wind speeds (U from 10 m) using **(b)** two different k values. The measured water and air values that were used to compute the concentration difference are shown in **(c)**. The bars across the top of the figure denote the different hydrographic regions discussed throughout the text.

fluxes remain low over the region. We do not observe any influence of atmospheric mixing ratios on the computed flux. Overall, we calculate that in high-wind-speed ($> 20\,\mathrm{m\,s^{-1}}$) areas, the different parameterizations have a large impact on the computed fluxes, and the k value should be considered more carefully in climatologies to avoid errors in the flux calculation.

We also compared our calculated flux results with the Lana climatology, and it can be seen from Fig. 9 that there are clear differences. The climatology shows lower results than those calculated from our observations in the subtropical region but higher values in the ACC region, at high latitudes ($> 43°$ S). The differences are due to differences in seawater concentrations used to calculate the fluxes, where our observations were slightly higher than in Lana et al. (2011) for parts of the subtropics and lower than in Lana et al. (2011) in the ACC. The subtropical region between 35 and 40° S, however, presents unexpected disagreement between the datasets, where the SCALE observations were similar to the climatology but the SCALE fluxes are obviously higher. This is due to the differences in wind speed encountered during our cruise in comparison to the monthly mean winds used in Lana et al. (2011). Finally, within the ACC region, the flux of DMS decreases rapidly, unlike the pattern displayed in the Lana climatology.
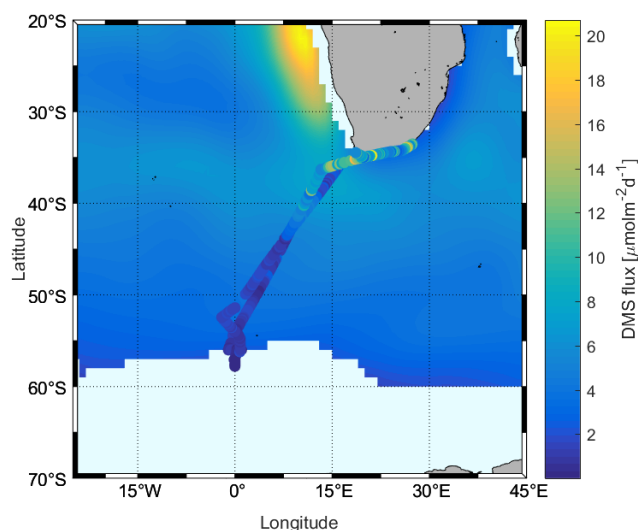

Figure 9. Comparison between calculated fluxes using N00 during the SCALE cruise (cruise track trace) and those in the Lana et al. (2011) climatology (background) for August.

3.6 Distribution of dissolved isoprene

In our study, we observed that the isoprene concentrations ranged from nd to $54.00\,\mathrm{pmol\,L^{-1}}$, and the average was $14.46 \pm 12.23\,\mathrm{pmol\,L^{-1}}$. These concentrations are within the range of published values (Table 2). Although our obser-
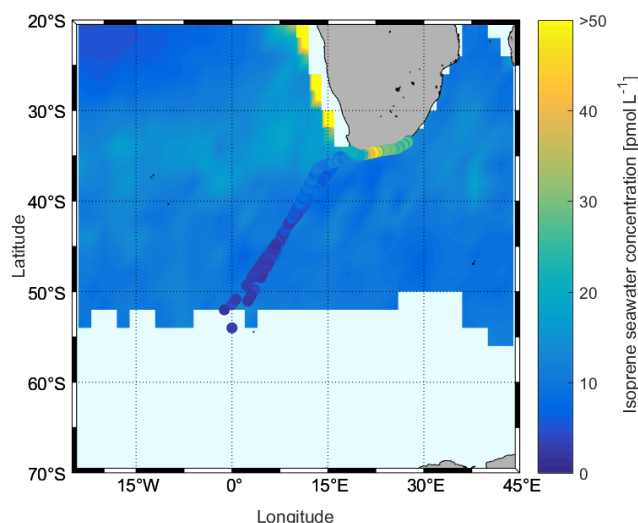
Figure 10. Comparison between measured sea surface isoprene concentrations during the SCALE cruise (cruise track trace) and those computed using a satellite-based model (Booge et al., 2016) for August 2019.

vation season is winter, on average, our measurements are not lower than those aboard the Antarctic Circumnavigation Expedition observed during December 2016–March 2017 on R/V *Akademik Tryoshnikov* (Rodríguez-Ros et al., 2020) and similar to the research cruise ANDREXII (Antarctic Deep Water Rates of Export) during autumn (February–April 2020) (Wohl et al., 2020). When we examine the different regions, we find the lowest isoprene concentrations in the Antarctic region (one data point only: $2.66\,\mathrm{pmol\,L^{-1}}$), followed by the ACC region (average: $3.76 \pm 1.46\,\mathrm{pmol\,L^{-1}}$, range: 2.06–$7.65\,\mathrm{pmol\,L^{-1}}$), with the highest concentrations in the subtropical region (average: $20.23 \pm 11.58\,\mathrm{pmol\,L^{-1}}$, range: 4.43–$54.00\,\mathrm{pmol\,L^{-1}}$). When we compare these regional values to previously published isoprene concentrations, it is obvious that wintertime concentrations are lower than other seasons (ACC vs. the R/V *Akademik Tryoshnikov* expedition). Results from a comparison with modeled surface isoprene concentrations (Booge et al., 2016) show that measured wintertime isoprene concentrations in the ACC and Antarctic regions are lower than expected (Fig. 10). Modeled isoprene concentrations in the open-ocean subtropical region agree with our measurements, whereas the model seems to underestimate surface isoprene concentrations in coastal areas. The results of measurements in the surface ocean during the stormy and mostly dark winter season in the Southern Ocean will be valuable for future atmospheric aerosol chemistry model studies, as they will not need to rely any longer on pure assumptions.

3.7 Isoprene air–sea fluxes

We calculated isoprene using two different gas exchange coefficient parameterizations, Wanninkhof (1992; W92) and Wanninkhof (2014; W14) (Fig. 11). We recommend using W14 to calculate fluxes of rather insoluble gases, as it is the updated version of W92 (based on later results). However, we use the W92 parameterization to compare to the isoprene flux model results from Booge et al. (2016). Generally, it can be seen that the k value has a large influence on the calculated fluxes. The values of kW92 are the highest (average: $30.43 \pm 20.74\,\mathrm{cm\,h^{-1}}$, range: 0.03–$143.18\,\mathrm{cm\,h^{-1}}$), but those of kW14 are within $17.64\,\%$ (average: $24.64 \pm 16.80\,\mathrm{cm\,h^{-1}}$, range: 0.03–$115.93\,\mathrm{cm\,h^{-1}}$). Values for kW14 in the subtropical, ACC, and Antarctic region are 26.88 ± 21.59, 25.01 ± 14.29, and $22.56 \pm 10.92\,\mathrm{cm\,h^{-1}}$, respectively. Values for kW92 are 33.20 ± 26.66, 30.88 ± 17.64, and $27.86 \pm 13.48\,\mathrm{cm\,h^{-1}}$, respectively. The differences between the two parameterizations are related to the magnitude of the coefficient, not the functional form of the wind speed dependence.

The computed isoprene flux ranged from nd to $407.05\,\mathrm{nmol\,m^{-2}\,d^{-1}}$, with an average of $80.55 \pm 78.57\,\mathrm{nmol\,m^{-2}\,d^{-1}}$. The average isoprene fluxes (ranges) in the subtropical, ACC, and Antarctic regions were 107.36 ± 84.30 (4.66–407.05) $\mathrm{nmol\,m^{-2}\,d^{-1}}$, 31.23 ± 26.85 (0.38–123.29) $\mathrm{nmol\,m^{-2}\,d^{-1}}$, and $18.03\,\mathrm{nmol\,m^{-2}\,d^{-1}}$ (one data point in Antarctic region), respectively. We observed that the isoprene fluxes can change rapidly and that changes in wind speed are the main factor driving the flux of isoprene, which is rather insoluble. This can be seen comparing isoprene concentrations and resulting fluxes during two time periods, DOYs 200–202 and 216–218, when passing through the same region (subtropical open-ocean region, Fig. 11). Isoprene concentrations were similar (8.01 ± 1.87 and $10.37 \pm 1.97\,\mathrm{pmol\,L^{-1}}$), but the fluxes from DOYs 216–218 are on average 3.9 times higher than during the time period DOYs 200–202. Isoprene fluxes fluctuated between 5.30 and $463.24\,\mathrm{nmol\,m^{-2}\,d^{-1}}$ in the coastal area and were influenced by varying surface isoprene concentrations and wind speed. However, it can be seen in the back trajectories (Fig. 1, right) that air masses from land reached coastal waters within a 24 h time period, which renders the assumption that the isoprene air mixing ratio is 0 unlikely. Thus, the flux values computed at the coast should be treated as upper limits.

Finally, we compared the results with Booge's model (background, Fig. 12). It can be seen that the overall model-based flux range is similar to the calculated fluxes using actual observations (Fig. 12). However, when comparing individual regions, we see that in the ACC and Antarctic region fluxes based on actual surface concentration measurements are lower than those predicted by the model. This is also true for some parts of the subtropical region, but variations are much higher, which also results in much higher isoprene fluxes than the Booge model, although the pattern is patchy.

Table 2. Isoprene seawater concentration observations in the Southern Ocean (SO).

Reference	Area	Time	Isoprene water (pmol L^{-1})	
			Mean	Range
Wohl et al. (2020)	SO	Autumn	13.4 ± 6.3	5.0–50.0
Rodríguez-Ros et al. (2020)	SO	Summer	10.7	2.1–88.4
Rodríguez-Ros et al. (2020)	SO and Weddell Sea	Summer	22.4	1.6–93.5
Rodríguez-Ros et al. (2020)	Southwestern Atlantic Shelf	Autumn	25.3	12.0–49.5
Kameyama et al. (2014)	SO	Summer	78.7	0.2–348
This study	SO: whole cruise	Winter	14.46 ± 12.23	nd–54.00
	SO: subtropical region		20.23 ± 11.58	4.42–54.00
	SO: ACC region		3.76 ± 1.46	2.06–7.65
	SO: Antarctic region		2.66	nd–2.66
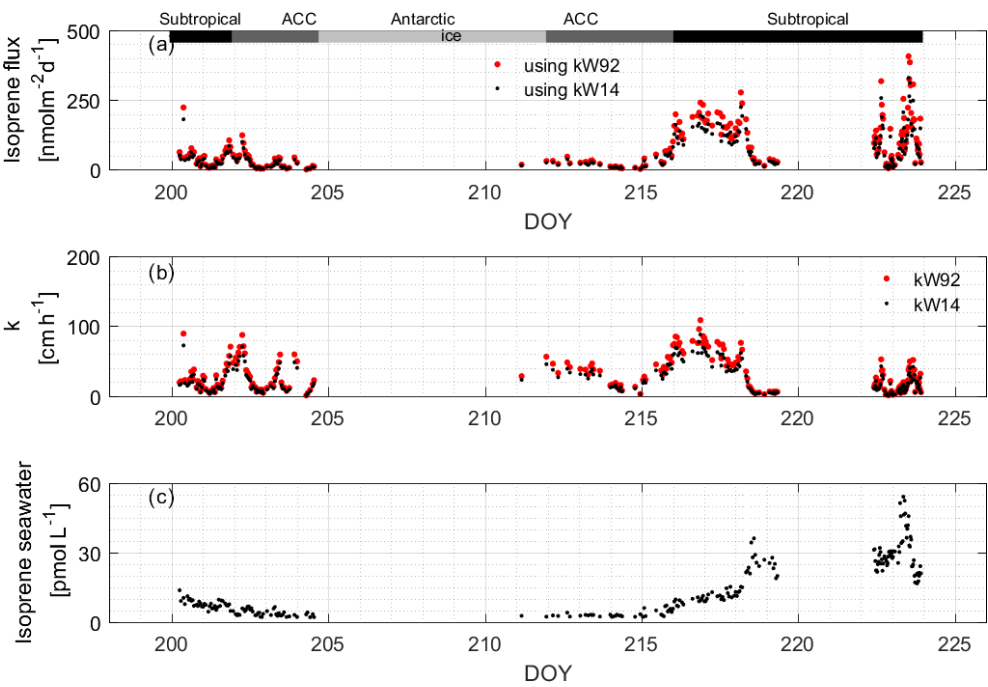
Figure 11. (a) Calculated isoprene fluxes using **(b)** two different k values. The measured water values that were used to compute the fluxes are shown in **(c)**. The bars across the top of the figure denote the different hydrographic regions discussed throughout the text.

In addition, in the northern ACC as well as in the subtropical region, the outbound and return travel areas are close together, but the fluxes span a wide range. The background value of the model is closer to the flux calculations on the outgoing trip, and the return trip is much higher than the outgoing trip, which is due to the change in wind speed.

4 Conclusions and outlook

DMS, DMSP, DMSO, and isoprene were observed in the surface waters (and DMS in the air) of the Southern Ocean during winter, where this type of data is severely limited. We found that all compounds in seawater showed a decreasing trend with latitude, while DMS in the atmosphere showed a maximum at high latitudes. The relationships between DMS, DMSP, and DMSO in distinct regions along the cruise track indicate that different processes are at work: there is no correlation among them in the Antarctic region but a positive correlation in lower–latitude regions. Especially in the subtropical regions, the different results in the coastal and open sea reflect the complex cycling between the three compounds, likely due to the influence of temperature and light. We found low DMS fluxes during the Southern Ocean winter season.
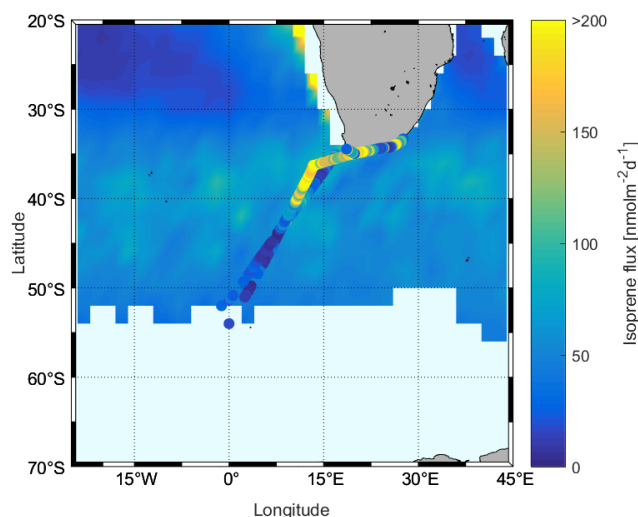
Figure 12. Comparison of calculated fluxes using W92 during the SCALE cruise (cruise track trace) and model-based fluxes using W92 from Booge et al. (2016) (background – monthly mean values of August 2019).

The calculated DMS fluxes using different k values suggest that previous studies might have overestimated the DMS flux.

Results of the first published isoprene winter values show that measured concentrations are lower than those computed by satellite-based model data. Furthermore, the mismatch between model results and field measurements clearly indicates the need for more field data in this region and season in order to develop better parameterizations for models. Our results also emphasize the need for temporally and seasonally highly resolved models. Due to its insolubility, isoprene fluxes are highly influenced by the magnitude of wind speed. Although isoprene concentrations in the open-ocean subtropical region were $10\,\mathrm{pmol\,L^{-1}}$ or lower, during high-wind-speed (DOYs 216–218) fluxes reached 100–$200\,\mathrm{nmol\,m^{-2}\,d^{-1}}$, which is significantly higher than coastal regions with low-wind-speed conditions and high oceanic isoprene concentrations ($\sim 30\,\mathrm{pmol\,L^{-1}}$). These small-scale variabilities are currently not captured using, e.g., monthly mean resolved models, which subsequently underestimates the influence of marine-derived isoprene on atmospheric processes. For both DMS and isoprene, the choice of k parameterization and the influence of wind speed on computed fluxes is important and should be treated with care.

Data products, such as monthly climatologies, are extremely important tools. It is apparent that more data during the winter season are needed to create a robust set of climate-active trace gas climatologies and process-based models. Undersampling can cause large uncertainties in the climatologies, model output, and computed parameters (Jiang, 2020; Vandemark et al., 2011; Wiggert et al., 1994). Given that changes in wind speed can be short term or have a long-term trend, it seems prudent to focus in the first place on obtain-ing robust maps of concentrations, perhaps at different time resolutions, that can be used with different wind products to compute fluxes. Furthermore, given that some trace gas databases (e.g., SOCAT; DMS PMEL, Pacific Marine Environment Laboratory) span decades, the data that are compiled into climatologies could reflect long-term trends that may need to be properly addressed. Finally, by comparing our measured field data with existing data products, some questions for future research emerge. How long-lived are fine spatial and temporal concentration/flux trends? How important (or misleading) are these finer-scale observations for creating monthly climatologies of trace gases? How do annual changes in wind speed influence climatological flux calculations, and how should this be reflected in new or updated climatologies? Future data-gathering campaigns are needed to answer these questions and create optimized data products.

References

Andreae, M. O.: Ocean-atmosphere interactions in the global biogeochemical sulfur cycle, Mar. Chem., 30, 1–29, https://doi.org/10.1016/0304-4203(90)90059-L, 1990.

Andreae, M. O. and Crutzen, P. J.: Atmospheric aerosols: Biogeochemical sources and role in atmospheric chemistry, Science, 276, 1052–1058, https://doi.org/10.1126/science.276.5315.1052, 1997.

Archer, S. D., Widdicombe, C. E., Tarran, G. A., Rees, A. P., and Burkill, P. H.: Production and turnover of particulate dimethylsulphoniopropionate during a coccolithophore bloom in the northern North Sea, Aquat. Microb. Ecol., 24, 225–241, https://doi.org/10.3354/ame024225, 2001.

Arneth, A., Monson, R. K., Schurgers, G., Niinemets, Ü., and Palmer, P. I.: Why are estimates of global terrestrial isoprene emissions so similar (and why is this not so for monoterpenes)?, Atmos. Chem. Phys., 8, 4605–4620, https://doi.org/10.5194/acp-8-4605-2008, 2008.

Arnold, S. R., Spracklen, D. V., Williams, J., Yassaa, N., Sciare, J., Bonsang, B., Gros, V., Peeken, I., Lewis, A. C., Alvain, S., and Moulin, C.: Evaluation of the global oceanic isoprene source and its impacts on marine organic carbon aerosol, Atmos. Chem. Phys., 9, 1253–1262, https://doi.org/10.5194/acp-9-1253-2009, 2009.

Baker, A. R., Turner, S. M., Broadgate, W. J., Thompson, A., McFiggans, G. B., Vesperini, O., Nightingale, P. D., Liss, P. S., and Jickells, T. D.: Distribution and sea-air fluxes of biogenic trace gases in the eastern Atlantic Ocean, Global Biogeochem. Cy., 14, 871–886, https://doi.org/10.1029/1999gb001219, 2000.

Bonsang, B., Polle, C., and Lambert, G.: Evidence for marine production of isoprene, Geophys. Res. Lett., 19, 1129–1132, https://doi.org/10.1029/92gl00083, 1992.

Booge, D., Marandino, C. A., Schlundt, C., Palmer, P. I., Schlundt, M., Atlas, E. L., Bracher, A., Saltzman, E. S., and Wallace, D. W. R.: Can simple models predict large-scale surface ocean isoprene concentrations?, Atmos. Chem. Phys., 16, 11807–11821, https://doi.org/10.5194/acp-16-11807-2016, 2016.

Booge, D., Schlundt, C., Bracher, A., Endres, S., Zäncker, B., and Marandino, C. A.: Marine isoprene production and consumption in the mixed layer of the surface ocean – a field study over two oceanic regions, Biogeosciences, 15, 649–667, https://doi.org/10.5194/bg-15-649-2018, 2018.

Bouillon, R.-C., Lee, P. A., de Mora, S. J., Levasseur, M., and Lovejoy, C.: Vernal distribution of dimethylsulphide, dimethylsulphoniopropionate, and dimethylsulphoxide in the North Water in 1998, Deep-Sea Res. Pt. II, 49, 5171–5189, https://doi.org/10.1016/S0967-0645(02)00184-4, 2002.

Broadbent, A. D., Jones, G. B., and Jones, R. J.: DMSP in corals and benthic algae from the Great Barrier Reef, Estuar. Coast. Shelf S., 55, 547–555, https://doi.org/10.1006/ecss.2002.1021, 2002.

Broadgate, W. J., Liss, P. S., and Penkett, S. A.: Seasonal emissions of isoprene and other reactive hydrocarbon gases from the ocean, Geophys. Res. Lett., 24, 2675–2678, https://doi.org/10.1029/97gl02736, 1997.

Broadgate, W. J., Malin, G., Kupper, F. C., Thompson, A., and Liss, P. S.: Isoprene and other non-methane hydrocarbons from seaweeds: a source of reactive hydrocarbons to the atmosphere, Mar. Chem., 88, 61–73, https://doi.org/10.1016/j.marchem.2004.03.002, 2004.

Cantoni, G. L. and Anderson, D. G.: Enzymatic cleavage of dimethylpropiothetin by polysiphonia lanosa, J. Biol. Chem., 222, 171–177, https://doi.org/10.1016/S0021-9258(19)50782-7, 1956.

Carpenter, L. J., Archer, S. D., and Beale, R.: Ocean-atmosphere trace gas exchange, Chem. Soc. Rev., 41, 6473–6506, https://doi.org/10.1039/C2CS35121H, 2012.

Cerqueira, M. and Pio, C.: Production and release of dimethylsulphide from an estuary in Portugal, Atmos. Environ., 33, 3355–3366, https://doi.org/10.1016/S1352-2310(98)00378-1, 1999.

Charlson, R. J., Lovelock, J. E., Andreae, M. O., and Warren, S. G.: Oceanic phytoplankton, atmospheric sulfur, cloud albedo and climate, Nature, 326, 655–661, https://doi.org/10.1038/326655a0, 1987.

Chen, Q., Sherwen, T., Evans, M., and Alexander, B.: DMS oxidation and sulfur aerosol formation in the marine troposphere: a focus on reactive halogen and multiphase chemistry, Atmos. Chem. Phys., 18, 13617–13637, https://doi.org/10.5194/acp-18-13617-2018, 2018.

Claeys, M., Graham, B., Vas, G., Wang, W., Vermeylen, R., Pashynska, V., Cafmeyer, J., Guyon, P., Andreae, M. O., Artaxo, P., and Maenhaut, W.: Formation of secondary organic aerosols through photooxidation of isoprene, Science, 303, 1173–1176, https://doi.org/10.1126/science.1092805, 2004.

Curran, M. A. and Jones, G. B.: Dimethyl sulfide in the Southern Ocean: Seasonality and flux, J. Geophys. Res.-Atmos., 105, 20451–20459, https://doi.org/10.1029/2000JD900176, 2000.

Curran, M. A. J., Jones, G. B., and Burton, H.: Spatial distribution of dimethylsulfide and dimethylsulfoniopropionate in the Australasian sector of the Southern Ocean, J. Geophys. Res.-Atmos., 103, 16677–16689, https://doi.org/10.1029/97jd03453, 1998.

Curson, A. R. J., Todd, J. D., Sullivan, M. J., and Johnston, A. W. B.: Catabolism of dimethylsulphoniopropionate: microorganisms, enzymes and genes, Nat. Rev. Microbiol., 9, 849–859, https://doi.org/10.1038/nrmicro2653, 2011.

Emerson, S., Stump, C., Wilbur, D., and Quay, P.: Accurate measurement of O_2, N_2, and Ar gases in water and the solubility of N_2, Mar. Chem., 64, 337–347, https://doi.org/10.1016/s0304-4203(98)00090-5, 1999.

Exton, D. A., Suggett, D. J., McGenity, T. J., and Steinke, M.: Chlorophyll-normalized isoprene production in laboratory cultures of marine microalgae and implications

for global models, Limnol. Oceanogr., 58, 1301–1311, https://doi.org/10.4319/lo.2013.58.4.1301, 2013.

Fiddes, S. L., Woodhouse, M. T., Nicholls, Z., Lane, T. P., and Schofield, R.: Cloud, precipitation and radiation responses to large perturbations in global dimethyl sulfide, Atmos. Chem. Phys., 18, 10177–10198, https://doi.org/10.5194/acp-18-10177-2018, 2018.

Gibson, J. A., Garrick, R. C., Burton, H. R., and McTaggart, A. R.: Dimethysulfide concentrations in the ocean close to the antarctic continent, Geomicrobiol. J., 6, 179–184, https://doi.org/10.1080/01490458809377837, 1988.

Guenther, A., Hewitt, C. N., Erickson, D., Fall, R., Geron, C., Graedel, T., Harley, P., Klinger, L., Lerdau, M., McKay, W. A., Pierce, T., Scholes, B., Steinbrecher, R., Tallamraju, R., Taylor, J., and Zimmerman, P.: A global model of natural volatile organic compound emissions, J. Geophys. Res.-Atmos., 100, 8873–8892, https://doi.org/10.1029/94jd02950, 1995.

Guenther, A., Karl, T., Harley, P., Wiedinmyer, C., Palmer, P. I., and Geron, C.: Estimates of global terrestrial isoprene emissions using MEGAN (Model of Emissions of Gases and Aerosols from Nature), Atmos. Chem. Phys., 6, 3181–3210, https://doi.org/10.5194/acp-6-3181-2006, 2006.

Guenther, A. B., Jiang, X., Heald, C. L., Sakulyanontvittaya, T., Duhl, T., Emmons, L. K., and Wang, X.: The Model of Emissions of Gases and Aerosols from Nature version 2.1 (MEGAN2.1): an extended and updated framework for modeling biogenic emissions, Geosci. Model Dev., 5, 1471–1492, https://doi.org/10.5194/gmd-5-1471-2012, 2012.

Hackenberg, S., Andrews, S. J., Airs, R., Arnold, S., Bouman, H., Brewin, R., Chance, R. J., Cummings, D., Dall'Olmo, G., and Lewis, A.: Potential controls of isoprene in the surface ocean, Global Biogeochem. Cy., 31, 644–662, https://doi.org/10.1002/2016GB005531, 2017.

Hatton, A. D., Darroch, L., and Malin, G.: The role of dimethylsulphoxide in the marine biogeochemical cycle of dimethylsulphide, Oceanogr. Mar. Biol. Ann. Rev., 42, 29–55, 2004.

Hatton, A. D., Shenoy, D. M., Hart, M. C., Mogg, A., and Green, D. H.: Metabolism of DMSP, DMS and DMSO by the cultivable bacterial community associated with the DMSP-producing dinoflagellate Scrippsiella trochoidea, Biogeochemistry, 110, 131–146, https://doi.org/10.1007/s10533-012-9702-7, 2012.

Hauck, J., Völker, C., Wang, T., Hoppema, M., Losch, M., and Wolf-Gladrow, D. A.: Seasonally different carbon flux changes in the Southern Ocean in response to the southern annular mode, Global Biogeochem. Cy., 27, 1236–1245, https://doi.org/10.1002/2013gb004600, 2013.

Houghton, J. T., Ding, Y., Griggs, D. J., Noguer, M., van der Linden, P. J., Dai, X., Maskell, K., and Johnson, C.: Climate Change 2001: The Scientific Basis. Contribution of Working Group I to the Third Assessment Report of the Intergovernmental Panel on Climate Change, The Press Syndicate of the University of Cambridge, United Kingdom and New York, NY, USA, 881 pp., 2001.

Hsu, S., Meindl, E. A., and Gilhousen, D. B.: Determining the power-law wind-profile exponent under near-neutral stability conditions at sea, J. Appl. Meteorol. Clim., 33, 757–765, https://doi.org/10.1175/1520-0450(1994)033<0757:DTPLWP>2.0.CO;2, 1994.

Hulswar, S., Simó, R., Galí, M., Bell, T. G., Lana, A., Inamdar, S., Halloran, P. R., Manville, G., and Mahajan, A. S.: Third revision of the global surface seawater dimethyl sulfide climatology (DMS-Rev3), Earth Syst. Sci. Data, 14, 2963–2987, https://doi.org/10.5194/essd-14-2963-2022, 2022.

Inomata, Y., Hayashi, M., Osada, K., and Iwasaka, Y.: Spatial distributions of volatile sulfur compounds in surface seawater and overlying atmosphere in the northwestern Pacific Ocean, eastern Indian Ocean, and Southern Ocean, Global Biogeochem. Cy., 20, GB2022, https://doi.org/10.1029/2005GB002518, 2006.

Jackson, R. L., Gabric, A. J., Cropp, R., and Woodhouse, M. T.: Dimethylsulfide (DMS), marine biogenic aerosols and the ecophysiology of coral reefs, Biogeosciences, 17, 2181–2204, https://doi.org/10.5194/bg-17-2181-2020, 2020.

Jiang, H.: Evaluation of altimeter undersampling in estimating global wind and wave climate using virtual observation, Remote Sens. Environ., 245, 111840, https://doi.org/10.1016/j.rse.2020.111840, 2020.

Jones, G. B., Curran, M. A., Swan, H. B., Greene, R. M., Griffiths, F. B., and Clementson, L. A.: Influence of different water masses and biological activity on dimethylsulphide and dimethylsulphoniopropionate in the subantarctic zone of the Southern Ocean during ACE 1, J. Geophys. Res.-Atmos., 103, 16691–16701, https://doi.org/10.1029/98JD01200, 1998.

Kameyama, S., Yoshida, S., Tanimoto, H., Inomata, S., Suzuki, K., and Yoshikawa-Inoue, H.: High-resolution observations of dissolved isoprene in surface seawater in the Southern Ocean during austral summer 2010–2011, J. Oceanogr., 70, 225–239, https://doi.org/10.1007/s10872-014-0226-8, 2014.

Keller, M. D., Bellows, W. K., and Guillard, R. R. L.: Dimethyl sulfide production in marine-phytoplankton, Acs Sym. Ser., 393, 167–182, https://doi.org/10.1021/bk-1989-0393.ch011, 1989.

Kettle, A. J., Andreae, M. O., Amouroux, D., Andreae, T. W., Bates, T. S., Berresheim, H., Bingemer, H., Boniforti, R., Curran, M. A. J., DiTullio, G. R., Helas, G., Jones, G. B., Keller, M. D., Kiene, R. P., Leck, C., Levasseur, M., Malin, G., Maspero, M., Matrai, P., McTaggart, A. R., Mihalopoulos, N., Nguyen, B. C., Novo, A., Putaud, J. P., Rapsomanikis, S., Roberts, G., Schebeske, G., Sharma, S., Simo, R., Staubes, R., Turner, S., and Uher, G.: A global database of sea surface dimethylsulfide (DMS) measurements and a procedure to predict sea surface DMS as a function of latitude, longitude, and month, Global Biogeochem. Cy., 13, 399–444, https://doi.org/10.1029/1999gb900004, 1999.

Kiene, R. P., Kieber, D. J., Slezak, D., Toole, D. A., del Valle, D. A., Bisgrove, J., Brinkley, J., and Rellinger, A.: Distribution and cycling of dimethylsulfide, dimethylsulfoniopropionate, and dimethylsulfoxide during spring and early summer in the Southern Ocean south of New Zealand, Aquat. Sci., 69, 305–319, https://doi.org/10.1007/s00027-007-0892-3, 2007.

Kloster, S., Feichter, J., Maier-Reimer, E., Six, K. D., Stier, P., and Wetzel, P.: DMS cycle in the marine ocean-atmosphere system – a global model study, Biogeosciences, 3, 29–51, https://doi.org/10.5194/bg-3-29-2006, 2006.

Koga, S., Nomura, D., and Wada, M.: Variation of dimethylsulfide mixing ratio over the Southern Ocean from 36° S to 70° S, Polar Sci., 8, 306–313, https://doi.org/10.1016/j.polar.2014.04.002, 2014.

Korhonen, H., Carslaw, K. S., Spracklen, D. V., Mann, G. W., and Woodhouse, M. T.: Influence of oceanic dimethyl sul-

fide emissions on cloud condensation nuclei concentrations and seasonality over the remote Southern Hemisphere oceans: A global model study, J. Geophys. Res.-Atmos., 113, D15204, https://doi.org/10.1029/2007jd009718, 2008.

Kulmala, M., Pirjola, U., and Makela, J. M.: Stable sulphate clusters as a source of new atmospheric particles, Nature, 404, 66–69, https://doi.org/10.1038/35003550, 2000.

Lana, A., Bell, T. G., Simo, R., Vallina, S. M., Ballabrera-Poy, J., Kettle, A. J., Dachs, J., Bopp, L., Saltzman, E. S., Stefels, J., Johnson, J. E., and Liss, P. S.: An updated climatology of surface dimethylsulfide concentrations and emission fluxes in the global ocean, Global Biogeochem. Cy., 25, GB1004, https://doi.org/10.1029/2010gb003850, 2011.

Laothawornkitkul, J., Taylor, J. E., Paul, N. D., and Hewitt, C. N.: Biogenic volatile organic compounds in the Earth system, New Phytol., 183, 27–51, https://doi.org/10.1111/j.1469-8137.2009.02859.x, 2009.

Lee, P. and De Mora, S.: DMSP, DMS and DMSO concentrations and temporal trends in marine surface waters at Leigh, New Zealand, in: Biological and environmental chemistry of DMSP and related sulfonium compounds, Springer, Boston, MA, https://doi.org/10.1007/978-1-4613-0377-0_34, 1996.

Lennartz, S. T., Marandino, C. A., von Hobe, M., Cortes, P., Quack, B., Simo, R., Booge, D., Pozzer, A., Steinhoff, T., Arevalo-Martinez, D. L., Kloss, C., Bracher, A., Röttgers, R., Atlas, E., and Krüger, K.: Direct oceanic emissions unlikely to account for the missing source of atmospheric carbonyl sulfide, Atmos. Chem. Phys., 17, 385–402, https://doi.org/10.5194/acp-17-385-2017, 2017.

Li, J. L., Zhai, X., Ma, Z., Zhang, H. H., and Yang, G. P.: Spatial distributions and sea-to-air fluxes of non-methane hydrocarbons in the atmosphere and seawater of the Western Pacific Ocean, Sci. Total Environ., 672, 491–501, https://doi.org/10.1016/j.scitotenv.2019.04.019, 2019.

Li, J. L., Zhai, X., Zhang, H. H., and Yang, G. P.: Temporal variations in the distribution and sea-to-air flux of marine isoprene in the East China Sea, Atmos. Environ., 187, 131–143, https://doi.org/10.1016/j.atmosenv.2018.05.054, 2018.

Liss, P. S.: Trace gas emissions from the marine biosphere, Philos. T. R. Soc. A, 365, 1697–1704, https://doi.org/10.1098/rsta.2007.2039, 2007.

Liss, P. S. and Slater, P. G.: Flux of gases across air-sea interface, Nature, 247, 181–184, https://doi.org/10.1038/247181a0, 1974.

Liss, P. S., Marandino, C. A., and Dahl, E. E.: Short-lived trace gases in the surface ocean and the atmosphere, in: Ocean-Atmosphere Interactions of Gases and Particles, Springer, Berlin, Heidelberg, 1–54, https://doi.org/10.1007/978-3-642-25643-1_1, 2014.

Lovelock, J. E., Maggs, R. J., and Rasmusse.Ra: Atmospheric dimethyl sulfide and natural sulfur cycle, Nature, 237, 452–453, https://doi.org/10.1038/237452a0, 1972.

Luis, A. J. and Lotlikar, V. R.: Hydrographic characteristics along two XCTD sections between Africa and Antarctica during austral summer 2018, Polar Sci., 30, 100705, https://doi.org/10.1016/j.polar.2021.100705, 2021.

Mahajan, A. S., Fadnavis, S., Thomas, M. A., Pozzoli, L., Gupta, S., Royer, S. J., Saiz-Lopez, A., and Simo, R.: Quantifying the impacts of an updated global dimethyl sulfide climatology on cloud microphysics and aerosol radiative forcing, J. Geophys. Res.-

Atmos., 120, 2524–2536, https://doi.org/10.1002/2014jd022687, 2015.

Mahmood, R., von Salzen, K., Norman, A.-L., Galí, M., and Levasseur, M.: Sensitivity of Arctic sulfate aerosol and clouds to changes in future surface seawater dimethylsulfide concentrations, Atmos. Chem. Phys., 19, 6419–6435, https://doi.org/10.5194/acp-19-6419-2019, 2019.

Matsunaga, S., Mochida, M., Saito, T., and Kawamura, K.: In situ measurement of isoprene in the marine air and surface seawater from the western North Pacific, Atmos. Environ., 36, 6051–6057, https://doi.org/10.1016/s1352-2310(02)00657-x, 2002.

McArdle, N., Liss, P., and Dennis, P.: An isotopic study of atmospheric sulphur at three sites in Wales and at Mace Head, Eire, J. Geophys. Res.-Atmos., 103, 31079–31094, https://doi.org/10.1029/98jd01664, 1998.

McGillis, W. R., Dacey, J. W. H., Frew, N. M., Bock, E. J., and Nelson, R. K.: Water-air flux of dimethylsulfide, J. Geophys. Res.-Oceans, 105, 1187–1193, https://doi.org/10.1029/1999jc900243, 2000.

McTaggart, A. R. and Burton, H.: Dimethyl Sulfide concentrations in the surface waters of the Australasian Antarctic and Subantarctic Oceans during an austral summer, J. Geophys. Res.-Oceans, 97, 14407–14412, https://doi.org/10.1029/92JC01025, 1992.

Milne, P. J., Riemer, D. D., Zika, R. G., and Brand, L. E.: Measurement of vertical-distribution of isoprene in surface seawater, its chemical fate, and its emission from several phytoplankton monocultures, Mar. Chem., 48, 237–244, https://doi.org/10.1016/0304-4203(94)00059-m, 1995.

Monson, R. K. and Holland, E. A.: Biospheric trace gas fluxes and their control over tropospheric chemistry, Annu. Rev. Ecol. Syst., 32, 547–576, https://doi.org/10.1146/annurev.ecolsys.32.081501.114136, 2001.

Moore, R. and Wang, L.: The influence of iron fertilization on the fluxes of methyl halides and isoprene from ocean to atmosphere in the SERIES experiment, Deep-Sea Res. Pt. II, 53, 2398–2409, https://doi.org/10.1016/j.dsr2.2006.05.025, 2006.

Mopper, K. and Kieber, D. J.: Photochemistry and the Cycling of Carbon, Sulfur, Nitrogen and Phosphorus, in: Biogeochemistry of Marine Dissolved Organic Matter, edited by: Hansell, D. A. and Carlson, C. A., chap. 9, Academic Press, San Diego, https://doi.org/10.1016/C2012-0-02714-7, 2002.

Naval Oceanographic Office: K10 Global 10 km Analyzed SST data set, Ver. 1.0, PO.DAAC, CA, USA, Naval Oceanographic Office [data set], https://doi.org/10.5067/GHK10-41N01 2008.

Nguyen, B., Mihalopoulos, N., and Belviso, S.: Seasonal variation of atmospheric dimethylsulfide at Amsterdam Island in the southern Indian Ocean, J. Atmos. Chem., 11, 123–141, https://doi.org/10.1007/BF00053671, 1990.

Nguyen, B., Mihalopoulos, N., Putaud, J., Gaudry, A., Gallet, L., Keene, W., and Galloway, J.: Covariations in oceanic dimethyl sulfide, its oxidation products and rain acidity at Amsterdam Island in the southern Indian Ocean, J. Atmos. Chem., 15, 39–53, https://doi.org/10.1007/BF0005360, 1992.

Nightingale, P. D., Malin, G., Law, C. S., Watson, A. J., Liss, P. S., Liddicoat, M. I., Boutin, J., and Upstill-Goddard, R. C.: In situ evaluation of air-sea gas exchange parameterizations using novel conservative and volatile tracers, Global Biogeochem. Cy., 14, 373–387, https://doi.org/10.1029/1999gb900091, 2000.

Ooki, A., Nomura, D., Nishino, S., Kikuchi, T., and Yokouchi, Y.: A global-scale map of isoprene and volatile organic iodine in surface seawater of the Arctic, Northwest Pacific, Indian, and Southern Oceans, J. Geophys. Res.-Oceans, 120, 4108–4128, https://doi.org/10.1002/2014jc010519, 2015.

Otte, M. L., Wilson, G., Morris, J. T., and Moran, B. M.: Dimethylsulphoniopropionate (DMSP) and related compounds in higher plants, J. Exp. Bot., 55, 1919–1925, https://doi.org/10.1093/jxb/erh178, 2004.

Palmer, P. I. and Shaw, S. L.: Quantifying global marine isoprene fluxes using MODIS chlorophyll observations, Geophys. Res. Lett., 32, L09805, https://doi.org/10.1029/2005gl022592, 2005.

Ryan-Keogh, T.: SCALE Winter SDS (1.0), Zenodo [data set], https://doi.org/10.5281/zenodo.6367853, 2022.

Rodríguez-Ros, P., Cortés, P., Robinson, C. M., Nunes, S., Hassler, C., Royer, S.-J., Estrada, M., Sala, M. M., and Simó, R.: Distribution and drivers of marine isoprene concentration across the Southern Ocean, Atmosphere, 11, 556, https://doi.org/10.3390/atmos11060556, 2020.

Sanchez, K. J., Chen, C. L., Russell, L. M., Betha, R., Liu, J., Price, D. J., Massoli, P., Ziemba, L. D., Crosbie, E. C., Moore, R. H., Muller, M., Schiller, S. A., Wisthaler, A., Lee, A. K. Y., Quinn, P. K., Bates, T. S., Porter, J., Bell, T. G., Saltzman, E. S., Vaillancourt, R. D., and Behrenfeld, M. J.: Substantial Seasonal Contribution of Observed Biogenic Sulfate Particles to Cloud Condensation Nuclei, Sci. Rep.-UK, 8, 3235, https://doi.org/10.1038/s41598-018-21590-9, 2018.

Sharkey, T. D., Wiberley, A. E., and Donohue, A. R.: Isoprene emission from plants: Why and how, Ann. Bot., 101, 5–18, https://doi.org/10.1093/aob/mcm240, 2008.

Shaw, S. L., Chisholm, S. W., and Prinn, R. G.: Isoprene production by Prochlorococcus, a marine cyanobacterium, and other phytoplankton, Mar. Chem., 80, 227–245, https://doi.org/10.1016/s0304-4203(02)00101-9, 2003.

Simó, R. and Vila-Costa, M.: Ubiquity of algal dimethyl-sulfoxide in the surface ocean: Geographic and temporal distribution patterns, Mar. Chem., 100, 136–146, https://doi.org/10.1016/j.marchem.2005.11.006, 2006.

Simó, R., Pedrós-Alió, C., Malin, G., and Grimalt, J. O.: Biological turnover of DMS, DMSP and DMSO in contrasting open-sea waters, Mar. Ecol.-Prog. Ser., 203, 1–11, https://doi.org/10.3354/meps203001, 2000.

Stefels, J., Steinke, M., Turner, S., Malin, G., and Belviso, S.: Environmental constraints on the production and removal of the climatically active gas dimethylsulphide (DMS) and implications for ecosystem modelling, Biogeochemistry, 83, 245–275, https://doi.org/10.1007/s10533-007-9091-5, 2007.

Thomas, M. A., Suntharalingam, P., Pozzoli, L., Rast, S., Devasthale, A., Kloster, S., Feichter, J., and Lenton, T. M.: Quantification of DMS aerosol-cloud-climate interactions using the ECHAM5-HAMMOZ model in a current climate scenario, Atmos. Chem. Phys., 10, 7425–7438, https://doi.org/10.5194/acp-10-7425-2010, 2010.

Tortell, P. D. and Long, M. C.: Spatial and temporal variability of biogenic gases during the Southern Ocean spring bloom, Geophys. Res. Lett., 36, L01603, https://doi.org/10.1029/2008gl035819, 2009.

Tran, S., Bonsang, B., Gros, V., Peeken, I., Sarda-Esteve, R., Bernhardt, A., and Belviso, S.: A survey of carbon monoxide and non-methane hydrocarbons in the Arctic Ocean during summer 2010, Biogeosciences, 10, 1909–1935, https://doi.org/10.5194/bg-10-1909-2013, 2013.

UK Met Office: OSTIA L4 SST Analysis (GDS2), Ver. 2.0, PO.DAAC, CA, USA, UK Met Office [data set], https://doi.org/10.5067/GHOST-4FK02, 2012.

Vallina, S. M. and Simó, R.: Strong relationship between DMS and the solar radiation dose over the global surface ocean, Science, 315, 506–508, https://doi.org/10.1126/science.1133680, 2007.

Van Alstyne, K. L.: The distribution of DMSP in green macroalgae from northern New Zealand, eastern Australia and southern Tasmania, J. Mar. Biol. Assoc. UK, 88, 799–805, https://doi.org/10.1017/s0025315408001562, 2008.

Vandemark, D., Salisbury, J. E., Hunt, C. W., Shellito, S. M., Irish, J., McGillis, W., Sabine, C., and Maenner, S.: Temporal and spatial dynamics of CO_2 air-sea flux in the Gulf of Maine, J. Geophys. Res.-Oceans, 116, C01012, https://doi.org/10.1029/2010JC006408, 2011.

Vogt, M. and Liss, P.: Dimethylsulfide and climate, Surface ocean-lower atmosphere processes, Anthropocene, 187, 197–232, https://doi.org/10.1016/j.ancene.2015.11.001, 2009.

von Glasow, R. and Crutzen, P. J.: Model study of multiphase DMS oxidation with a focus on halogens, Atmos. Chem. Phys., 4, 589–608, https://doi.org/10.5194/acp-4-589-2004, 2004.

Wanninkhof, R.: Relationship between wind speed and gas exchange over the ocean, J. Geophys. Res.-Oceans, 97, 7373–7382, https://doi.org/10.1029/92JC00188, 1992.

Wanninkhof, R.: Relationship between wind speed and gas exchange over the ocean revisited, Limnol. Oceanogr.-Meth., 12, 351–362, https://doi.org/10.4319/lom.2014.12.351, 2014.

Went, F. W.: Blue Hazes in the Atmosphere, Nature, 187, 641–643, https://doi.org/10.1038/187641a0, 1960.

Wiggert, J., Dickey, T., and Granata, T.: The effect of temporal undersampling on primary production estimates, J. Geophys. Res.-Oceans, 99, 3361–3371, https://doi.org/10.1029/93JC03163, 1994.

Wohl, C., Brown, I., Kitidis, V., Jones, A. E., Sturges, W. T., Nightingale, P. D., and Yang, M.: Underway seawater and atmospheric measurements of volatile organic compounds in the Southern Ocean, Biogeosciences, 17, 2593–2619, https://doi.org/10.5194/bg-17-2593-2020, 2020.

Yang, J. and Yang, G.-P.: Distribution of dissolved and particulate dimethylsulfoxide in the East China Sea in winter, Mar. Chem., 127, 199–209, https://doi.org/10.1016/j.marchem.2011.09.006, 2011.

Yang, M., Blomquist, B., Fairall, C., Archer, S., and Huebert, B.: Air-sea exchange of dimethylsulfide in the Southern Ocean: Measurements from SO GasEx compared to temperate and tropical regions, J. Geophys. Res.-Oceans, 116, C00F05, https://doi.org/10.1029/2010JC006526, 2011.

Yoch, D. C.: Dimethylsulfoniopropionate: Its sources, role in the marine food web, and biological degradation to dimethylsulfide, Appl. Environ. Microbiol., 68, 5804–5815, https://doi.org/10.1128/aem.68.12.5804-5815.2002, 2002.

Zavarsky, A., Goddijn-Murphy, L., Steinhoff, T., and Marandino, C. A.: Bubble-Mediated Gas Transfer and Gas Transfer Suppression of DMS and CO2, J. Geophys. Res.-Atmos., 123, 6624–6647, https://doi.org/10.1029/2017jd028071, 2018.

Zhang, M., Marandino, C. A., Chen, L., Sun, H., Gao, Z., Park, K., Kim, I., Yang, B., Zhu, T., and Yan, J.: Characteristics of the surface water DMS and pCO$_2$ distributions and their relationships in the Southern Ocean, southeast Indian Ocean, and northwest Pacific Ocean, Global Biogeochem. Cy., 31, 1318–1331, https://doi.org/10.1002/2017GB005637, 2017.

Zhang, M., Park, K.-T., Yan, J., Park, K., Wu, Y., Jang, E., Gao, W., Tan, G., Wang, J., and Chen, L.: Atmospheric dimethyl sulfide and its significant influence on the sea-to-air flux calculation over the Southern Ocean, Prog. Oceanogr., 186, 102392, https://doi.org/10.1016/j.pocean.2020.102392, 2020.

Zhang, M. M., Gao, W., Yan, J. P., Wu, Y. F., Marandino, C. A., Park, K., Chen, L. Q., Lin, Q., Tan, G. B., and Pan, M. J.: An integrated sampler for shipboard underway measurement of dimethyl sulfide in surface seawater and air, Atmos. Environ., 209, 86–91, https://doi.org/10.1016/j.atmosenv.2019.04.022, 2019.

Zhou, L., Booge, D., Zhang, M., and Marandino, C. A.: Winter time trace gas concentrations during SCALE in 2019, Zenodo [data set], https://doi.org/10.5281/zenodo.7185513, 2022.

Zindler, C., Bracher, A., Marandino, C. A., Taylor, B., Torrecilla, E., Kock, A., and Bange, H. W.: Sulphur compounds, methane, and phytoplankton: interactions along a north–south transit in the western Pacific Ocean, Biogeosciences, 10, 3297–3311, https://doi.org/10.5194/bg-10-3297-2013, 2013.

Zindler, C., Lutterbeck, H., Endres, S., and Bange, H. W.: Environmental control of dimethylsulfoxide (DMSO) cycling under ocean acidification, Environ. Chem., 13, 330–339, https://doi.org/10.1071/EN14270, 2015.

Zindler, C., Marandino, C. A., Bange, H. W., Schutte, F., and Saltzman, E. S.: Nutrient availability determines dimethyl sulfide and isoprene distribution in the eastern Atlantic Ocean, Geophys. Res. Lett., 41, 3181–3188, https://doi.org/10.1002/2014gl059547, 2014.

Zubkov, M. V., Fuchs, B. M., Archer, S. D., Kiene, R. P., Amann, R., and Burkill, P. H.: Rapid turnover of dissolved DMS and DMSP by defined bacterioplankton communities in the stratified euphotic zone of the North Sea, Deep-Sea Res. Pt. II, 49, 3017–3038, https://doi.org/10.1016/s0967-0645(02)00069-3, 2002.